

THE CALCULATION OF AUTOIONIZATION POSITIONS AND WIDTHS WITH
APPLICATIONS TO PENNING IONIZATION REACTIONS

BY

Alan David Isaacson

Materials and Molecular Research Division
Lawrence Berkeley Laboratory
University of California
Berkeley, California 94720

ABSTRACT

The Calculation of Autoionization Positions and Widths with Applications to Penning Ionization Reactions

by

Alan David Isaacson

Using an approximate evaluation of Miller's golden rule formula to calculate autoionization widths which allows for the consideration only of L^2 functions, the positions and lifetimes of the lowest $1,3P$ autoionizing states of He have been obtained to reasonable accuracy. This method has been extended to molecular problems, and the ab initio configuration interaction potential energy and width surfaces for the $\text{He}(2^3S)+\text{H}_2$ system have been obtained. Quantum mechanical close-coupling calculations of ionization cross sections using the complex $V^* - \frac{i}{2}\Gamma$ potential have yielded rate constants in good agreement with the experimental results of Lindinger, et al. The potential energy surface of the $\text{He}(2^1S)+\text{H}_2$ system has also been obtained, and exhibits not only a high degree of anisotropy, but also contains a relative maximum for a perpendicular (C_{2v}) approach which appears to arise from s-p hybridization of the outer He orbital. However, similar ab initio calculations on the $\text{He}(2^1S)+\text{Ar}$ system do not show such anomalous structure. In addition, the complex poles of the S-matrix (Siebert eigenvalues) have been calculated for several autoionizing states of He and H^- , with

encouraging results even for quite modest basis sets. This method has been extended to molecular problems, and results have been obtained for the $\text{He}(2^3\text{S})+\text{H}$ and $\text{He}(2^1\text{S})+\text{H}$ systems.

To my wife, Lisa

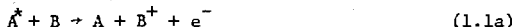
TABLE OF CONTENTS

	Page
Abstract	1
I. Introduction	1
II. Preliminary Atomic Calculations	6
A. Theoretical Considerations	6
B. Results for $\text{He}(2s2p^{1,3}P)$	9
III. The Extension of an Approximate Golden Rule Method to Molecular Calculations	16
IV. The $\text{He}(2^3S)+\text{H}_2$ System: Potential Energy and Width Surfaces	24
V. Scattering Calculations on the $\text{He}(2^3S)+\text{H}_2$ System	46
A. Quantum Mechanical Calculations	47
1. Theoretical Considerations	47
2. Results	52
B. Classical Calculations	62
1. Theory	62
2. Results	68
VI. The $\text{He}(2^1S)+\text{H}_2$ System	79
VII. The $\text{He}(2^1S)+\text{Ar}$ System	94
VIII. The Calculation of Siegert Eigenvalues	109
A. The Variational Calculation of Siegert Eigenvalues	111
B. The Calculation of Atomic Resonances and Results	119
C. The Application to Molecular Systems: Results for $\text{He}(2^{1,3}S)+\text{H}$	126

	Page
Acknowledgments143
References144

1. INTRODUCTION

Penning ionization is the collisional autoionization of a two particle system A^*-B , in which the excitation energy of particle A is greater than the ionization potential of particle B:



(Actually, reaction (1.1a) is referred to as Penning ionization, while reaction (1.1b) is often called associative ionization.) These reactions play an important role in many phenomena, such as gaseous discharges, shock waves, photolysis, and plasmas. In fact, Penning ionization involving He atoms in the lowest metastable states is important in the physics of the atmosphere of stars and planets.

Under the Born-Oppenheimer approximation, we can separate the electronic problem of the ionization from the nuclear motion. Thus, for a given (fixed) nuclear geometry, the (electronically) bound A^*-B state is sitting in a continuum of $A-B^+ + e^-$ states, since the energy of the ejected electron is not quantized. From quantum mechanics, however, we know that in such a situation, the bound state rapidly decays to the continuum, with a lifetime on the order of 10^{-13} sec. A way to view this decay is as follows: For energies close to the resonance energy $E_r > 0$, the eigensolutions have large amplitudes for a bound A^*-B configuration near the nuclei, but asymptotically behave like oscillatory continuum solutions.¹ If we imagine that at time $t=0$ we form the system in the bound state, then this corresponds to a linear combination of

eigenfunctions in which all of the asymptotic oscillations interfere destructively. However, at some later time (still with fixed nuclei), this linear combination of eigensolutions changes, and thus the asymptotic oscillations grow, corresponding to a net outward flux of ionized electrons.

Within a classical or semiclassical framework, all of the interesting aspects of the dynamics--ionization cross sections, branching ratios for associative to Penning ionization, the angular distributions of both electrons and heavy particles, and the energy distribution of the ionized electrons--are determined by the three functions V^* , V_+ , and Γ . V^* and V_+ are the potential energy surfaces for the A^*-B and $A-B^+$ systems, respectively, while Γ is the width, or probability of ionization, as a function of nuclear coordinates. (Alternatively, Γ/h is the autoionization rate, while h/Γ is the lifetime of the A^*-B state with respect to autoionization.) The present work deals mainly with the calculation of these three functions.

Since $A-B^+$ is an ordinary bound electronic state, the V_+ surface can easily be obtained with standard techniques of electronic structure calculations. However, since the A^*-B state is imbedded in a continuum of ionized states, other techniques are necessary for the calculation of V^* and Γ . V^* can often be calculated with relative ease by using the stabilization method.²⁻⁵ In practice, this method reduces to a variational calculation in which the trial wavefunction is restricted to those configurations which one intuitively assumes should contribute most to the bound part of the resonant eigenfunction. The form of this trial function is also chosen to decay asymptotically, so that bound state techniques (e.g., integrals over orbitals and matrix diagonalization) may be applied without modification. The calculation of the width is much less straightforward. One method which has been relatively successful

employs the golden rule approximation of Miller.⁶ Using Feshbach projection operator techniques,⁷ Miller found that the width is given by (in atomic units)

$$\Gamma = 2\pi \rho |\langle \phi | H - E_r | \chi \rangle|^2, \quad (1.2)$$

where ϕ is a normalized bound state wavefunction describing the metastable A-B state, χ is a continuum function degenerate with ϕ which describes the ionized A-B⁺ + e⁻ state, and ρ is the density of continuum states at E_r , the resonance energy:

$$E_r = \langle \phi | H | \phi \rangle. \quad (1.3)$$

This result suggests that we may view the width as the square of the coupling matrix element between an initial (bound) and final (continuum) state, in analogy to the standard result from time-dependent perturbation theory.⁸ (The $-E_r \langle \phi | \chi \rangle$ term of Eq. (1.2) results from orthogonalization of χ to ϕ .)

A more direct method of determining V^* and Γ which recently has shown great promise is a variational calculation of the Siegert eigenvalues of the system.⁹⁻¹¹ These eigenvalues correspond to complex energies at which the Green's function or, equivalently, the S-matrix, has poles. These occur at the resonances of the system as well as at the bound states. Physically, the pole in the S-matrix for a resonance arises because there is only an outward flux of electrons from the autoionizing state. Since these poles occur energies $E_r - \frac{i}{2} \Gamma$, we obtain both V^* and Γ from the same calculation.

Until fairly recently, Γ had been obtained only for two and three electron systems.^{12,13} However, these calculations employed the golden

rule approach, and involved procedures, such as the use of Hylleraas basis sets or the evaluation of matrix elements between bound and continuum functions, which cannot easily be extended to more complicated systems. Another approach, the method of rotated coordinates, has also been used successfully for calculations on small atomic systems,¹⁴ and appears to be well suited to problems with spherical symmetry. However the extension to non-spherically symmetric problems, i.e., molecules, is not clear. Therefore, the goal of the work presented in this thesis has been to develop simple methods for the calculations of autoionization energies and widths which are based on standard electronic structure techniques, and which can be applied to larger, molecular systems. Of particular emphasis in this work have been systems which involve the lowest $1,^3S$ states of He colliding with various targets (e.g., H, H₂, and Ar). These systems were chosen for a number of reasons: (1) There are relatively few electrons, so that rather extensive electronic structure calculations are feasible. (2) It is possible, once the potential energy surfaces and widths are available, to obtain cross-section information for these systems fairly easily, which can then be compared with experiment. (3) Reliable experimental data are available on these systems. (4) Experimental results on the He(2^1S)+H₂, Ar systems have indicated that the corresponding potential curves contain relative maxima,¹⁵⁻¹⁷ a rather unusual feature.

The following chapters contain the implementation of both the stabilization--golden rule and Siegert eigenvalue approaches outlined above. Chapter II contains a preliminary calculation of some He resonances by an approximate version of the golden rule method, in which the continuum function χ of Eq. (1.2) is replaced by a function which asymptotically decays. The extension of this method to molecular calculations

is discussed in Chapter III, and results for the potential energy surfaces and widths for the $\text{He}(2^3\text{S})+\text{H}_2$ system are presented in Chapter IV. In Chapter V, both quantum mechanical and classical scattering calculations of the ionization cross sections and rate constants for the $\text{He}(2^3\text{S})+\text{H}_2$ system are discussed, and shown to be in good agreement with experiment, thus demonstrating that the surfaces and widths are reasonably accurate. Chapters VI and VII present our results for the potential energy surfaces of the $\text{He}(2^1\text{S})+\text{H}_2$ and $\text{He}(2^1\text{S})+\text{Ar}$ systems, respectively. The former is shown to contain an anomalous structure for certain geometries, while the latter does not. Finally, the calculations of the Siegert eigenvalues for both atomic and molecular systems are discussed in Chapter VIII, and the results for the $\text{He}(2^3\text{S})+\text{H}$ and $\text{He}(2^1\text{S})+\text{H}$ systems are presented.

II. PRELIMINARY ATOMIC CALCULATIONS

In order to study the feasibility of approximating the continuum function γ in the golden rule formula [Eq. (1.2)] by a function which asymptotically decays, calculations have been performed for the positions and widths of two autoionizing states of He.¹⁹ Section A discusses the theoretical aspects of the calculation. Results for the He(2s2p^{1,3}P) autoionizing states are presented in Section B, and compared with more accurate calculations of Miller⁶ and Bhatia and Temkin.¹²

A. Theoretical Considerations

The motivation for the idea of this approximation lies in the fact that the bound function ϕ used in Eq. (1.2) decays rapidly to zero outside of a region of space near the nucleus. This implies that we only get contributions to the width inside of this region, and we therefore only need to know the form of the continuum function χ of Eq. (1.2) inside this region. Thus, χ can be approximated by a function which also decays asymptotically, i.e., χ can be taken as a linear combination of some set of square-integrable (L^2) functions, as long as this set spans a region of space at least as large as that spanned by ϕ . (Furthermore, since ϕ approximates the exact resonant eigenfunction in the region of configuration space characterizing the metastable state, the quantity $(H-E_r)\phi$ is approximately zero. Therefore, the form of χ is actually important only in some "shell" near the extent of ϕ .)

As will soon become clear, a convenient choice for this approximate χ is one of the non-resonant eigenfunctions of the Hamiltonian matrix used in the stabilization procedure. For, following Hazi and Taylor's analysis of a one-dimensional model problem,² when we performed a stabilization

calculation, we start with some basis of N orthonormal spin configurations $\{\psi_i\}$ and diagonalize the Hamiltonian matrix

$$H_{ij} = \langle \psi_i | H | \psi_j \rangle \quad . \quad (2.1)$$

On physical grounds, we can then identify one root as the resonance:

$$\psi_r = \sum_{i=1}^N a_{ri} \psi_i \quad , \quad (2.2)$$

and obtain the resonance position:

$$E_r = \langle \psi_r | H | \psi_r \rangle \quad . \quad (2.3)$$

In addition, as Hazi and Taylor demonstrate,² some of the other $N-1$ eigenfunctions of H_{ij} are approximate "continuum-like" solutions of energy E_c that correspond to the ionized state $\text{He}^+ + e^-$ for various electron energies:

$$\chi_c = \sum_{i=1}^N a_{ci} \psi_i \quad . \quad (2.4)$$

These approximate solutions oscillate within the space spanned by the basis set, but decay rapidly to zero outside of this space. But since this space is the same as that over which ψ_r is defined, approximating χ of Eq. (1.2) by one of the χ_c having the proper energy should still provide a reasonable result for the width.

A further consideration is that ψ_r of Eq. (2.2) also contains contributions from configurations which correspond to continuum-like solutions. To get a bound function ϕ for the golden rule expression,

then, we must first project out of ψ_r these continuum contributions. This is easily done by restricting the summation in Eq. (2.2) to exclude these continuum configurations. This then provides us with our approximate ϕ :

$$\phi \approx \sum_{i=1}^{N'} a_{ri} \phi_i \quad , \quad (2.5)$$

where the prime on the summation indicates the exclusion of certain configurations. (Note that if this projection is not done, the orthogonality of ψ_r and χ_c would give a zero width.) Substituting the approximate χ and ϕ choices of Eqs. (2.4) and (2.5) into the golden rule formula (1.2), and using the fact that

$$H \chi_c = E_c \chi_c \quad , \quad (2.6)$$

we trivially obtain our working equation for the width:

$$\Gamma = 2\pi\rho (E_r - E_c)^2 \left| \sum_{i=1}^{N'} a_{ri} a_{ci} \right|^2 \quad , \quad (2.7)$$

where the prime emphasizes that the summation excludes certain configurations.

Before using Eq. (2.7), however, we must first determine ρ , the density of continuum states at the resonance energy. As discussed above, χ_c decays rapidly at the boundary of the space spanned by the basis set. This roughly corresponds to the boundary condition of an infinite wall at some boundary L , so that we may use a particle-in-a-box analysis to claim that the energies of continuum states corresponding to $\text{He}^+ + e^-$ which are determined by the basis set are roughly given by (in atomic units)

$$E_n = -\frac{1}{2} Z^2 + \frac{1}{2} k_n^2 \quad , \quad (2.8)$$

where $-\frac{1}{2} Z^2$ is the energy of the He^+ core and k_n is given by

$$k_n \approx 2\pi n/L \quad . \quad (2.9)$$

This analysis is substantiated by the fact that when k_n is determined for each continuum eigenvalue, a k_n vs n plot is nearly linear. From Eq. (2.8), it is clear that

$$\frac{\partial E_n}{\partial n} = k_n \frac{\partial k_n}{\partial n} \quad , \quad (2.10)$$

or, for a unit change in n ,

$$\Delta E_n \approx k_n \Delta k \quad . \quad (2.11)$$

However, since the eigenfunctions are normalized to unity by the stabilization procedure, we can take

$$\rho = \frac{1}{\Delta E} \approx \frac{1}{k_n \Delta k} \quad . \quad (2.12)$$

The slope Δk of the k_n vs n plot can be determined to an accuracy of 10-15%, causing a corresponding uncertainty in ρ .

B. Results for $\text{He}(2s2p^1, 3P)$

The positions and widths of the $2s2p^1, 3P$ autoionizing states of He were calculated using the HETINT and MRINO programs written by Schaefer.²⁰ The basis sets for these calculations were composed of linear combinations of Slater determinants formed from Slater type orbitals with exponents

given in Table I. (Each orbital in this list is orthogonalized to those preceding it.) The 2s and 2p exponents were chosen by optimizing the energy of the autoionizing state in a separate calculation consisting only of the 1s2p and 2s2p configurations. A set of diffuse p functions was then added to represent an oscillatory continuum orbital. (The rather large exponent for this p set was chosen so that the outermost maxima of the radial p functions roughly matched the extrema of a radial coulomb function of the proper energy.)

From the orbital basis in Table I, 1s2p and 2s2p configurations were chosen to represent the bound resonant state, and a set of 1s2p', 1s3p, ..., 1s8p configurations was taken to represent various continuum solutions. That is, since these configurations roughly correspond to a bound 1s electron and a p electron with large amplitude far from the nucleus, a linear combination of such 1snp configurations should approximate the He^+e^- state. Configuration interaction (CI) calculations were then performed with this set of 9 configurations. Since only the 1s2p and 2s2p configurations were chosen to describe the resonance, the primed summation in Eq. (2.7) consists only of two terms. Γ is thus not only very simple to evaluate, but is also a direct measure of the amount that the resonant state mixes into the continuum state, and vice-versa.

It was initially hoped that the resonant root would be closely bracketed by continuum-like solutions, providing (approximately) the degeneracy to ϕ required by the golden rule formula and allowing for the computation of an average width. However, since adjacent continuum solutions differ (roughly) by one-half of a wavelength over the effective length of the "box" formed by the basis set (see Section A), these

Table I. Basis sets for atomic calculations.

	3_p	1_p
1s	$Z = 2.00$	$Z = 2.00$
2s	.74	.56
2p	.85	.99
$2p^7, 3p-8p$	1.71 - 1.81	1.71 - 1.81

Figure I. Γ for He(3P) resonance as determined from the golden rule equation (2.7) for several basis sets giving continuum roots in a range near the resonance energy $E_r = -0.7504$ a.u.

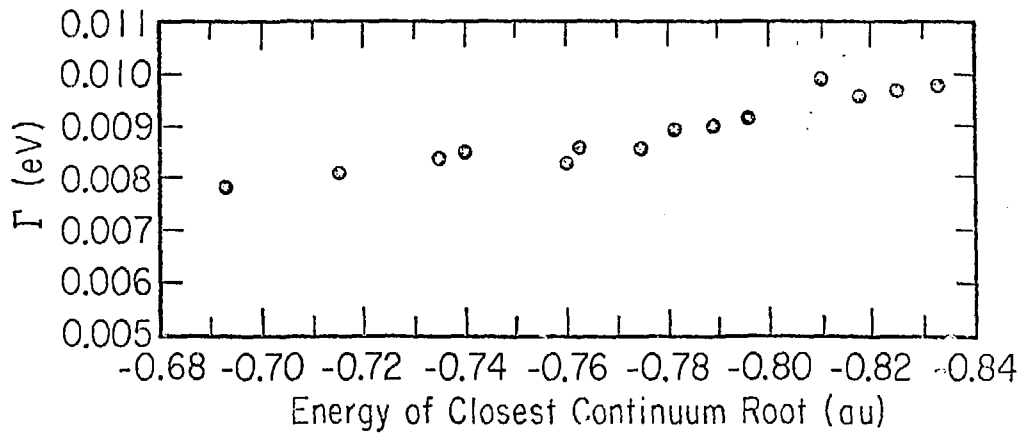


Figure I.

solutions are widely spaced. It was possible, though, by adjusting the exponent ζ of the $2p'-3p$ set, to get one continuum-like solution fairly close to resonance. In fact, as ζ was varied, the energy E_c of the closest continuum root moved monotonically through an interval about E_r . The width Γ was then calculated for a number of E_c values. Since both Γ and E_r were relatively stable against variations in ζ , $\Gamma(E_c)$ values could easily be interpolated for a value at $E_c = E_r$. Results for Γ as a function of E_c are plotted in Figure I for the $\text{He}(^3P)$ resonance. Final interpolated results for the positions and widths of the $^1,^3P$ resonances are given in Table II, and compared with the more accurate golden rule calculations of Miller,⁶ and with the accurate Feshbach projection operator calculations of Bhatia and Temkin.¹² The agreement in the 1P widths is quite good, while our 3P width is about a factor of two too large. From the crudeness of the approximations described above, however, even an error of a factor of two is quite reasonable. It is also important to note here that good results can be obtained for the widths even though the errors in the resonance energies are quite large. Of course, the resonance energies could be improved by performing larger CI calculations, but the interest here was in determining if reasonable widths could be obtained with a small enough basis such that the method presented above could be applied to larger systems, as will be discussed in the following chapters.

Table II. Final results for atomic resonances.

State	This Work		Miller's Results ^a		Accurate Values ^b	
	E_r (a.u.)	Γ (eV)	E_r (a.u.)	Γ (eV)	E_r (a.u.)	Γ (eV)
He(2^1P)	-0.6577	0.0420	-0.6579	0.0375	-0.6929	0.0374
He(2^3P)	-0.7504	0.0170	-0.7531	0.0078	-0.7615	0.0084

^aSee References 6

^bSee References 12.

III. THE EXTENSION OF AN APPROXIMATE GOLDEN RULE METHOD TO MOLECULAR CALCULATIONS

In the preceding chapter, we demonstrated that one could obtain reasonable results for the width of an autoionizing state even when the continuum function χ in the golden rule formula [Eq. (1.2)] is replaced by a function which asymptotically decays. However, the procedure discussed above possesses several serious drawbacks, prohibiting a direct application to molecular systems. First, the method is not accurate enough for quantitative calculations. Second, the need for running several calculations with different basis sets would make the method too costly. Finally, the procedure requires the identification of a "continuum-like" eigensolution, which is difficult, if not impossible, for larger, molecular systems.

These drawbacks can be eliminated, however, by a more accurate (but still practical) choice for the continuum function χ . For, with only a different choice for χ (involving the true coulomb orbital for the ionized electron), Miller⁶ obtained very accurate widths for the atomic systems discussed in Chapter II (cf. Table II). The major problem with such a choice for χ , though, is that the matrix element evaluations required by the golden rule formula are too time-consuming for general application to larger systems. The basic idea of the approach developed in this chapter, then, is to explicitly expand this coulomb orbital in a set of square-integrable functions. As we shall see, this leads to a practical way of defining the P and Q projection operators of the Feshbach approach⁷ such that standard configuration interaction (CI) techniques can be used with almost no modifications. Application of

of this method to the $\text{He}(2^3\text{S})+\text{H}_2$ system¹ is presented in Chapter IV.

As before, let H be the electronic Hamiltonian for an autoionization problem with N electrons. (The nuclear geometry \bar{R} is fixed and suppressed.) As discussed in Chapter V, the resonance eigenfunction of H has two different components,¹ one which resembles a purely bound state and another which resembles the product of an $N-1$ electron ion core wavefunction and a function which asymptotically behaves like a coulomb wave. Now suppose we choose an orthonormal set of L^2 spatial orbitals $\{\phi_1, \dots, \phi_n\}$ which is flexible enough to represent both the bound and the ionized components of the resonant eigenfunction in some finite region of space. We then construct orthonormal configurations $\{\psi_i\}$ by taking linear combinations of Slater determinants formed from this orbital set which have the proper spatial symmetry. This set of orthonormal configurations $\{\psi_i\}$ forms the basis for a space \hat{A} of N electron wavefunctions, where \hat{A} is a subspace of A , the space of all possible N electron wavefunctions. Let us next denote by \hat{H} the representation of H in this space \hat{A} . That is,

$$\hat{H} = \sum_{ij} |\phi_i\rangle H_{ij} \langle\phi_j| \quad (3.1)$$

where

$$H_{ij} = \langle\phi_i|H|\phi_j\rangle \quad (3.2)$$

We now wish to partition the space \hat{A} such that we can identify the bound and ionized components of the eigenfunctions of \hat{H} . For this purpose, let ψ_{ion} be an approximate wavefunction for the ground state of the $N-1$ electron ion core which has been constructed from the $\{\phi_i\}$ set,

and let us define

$$\chi_i = A \psi_{\text{ion}}(\vec{r}_1, \dots, \vec{r}_{N-1}) \phi_i(\vec{r}_N) \quad , \quad i = 1, \dots, n \quad , \quad (3.3)$$

where A is the antisymmetrizer. Then each χ_i has the form of an ion core times another orbital, and since ψ_{ion} has been constructed from the $\{\phi_i\}$ set, each χ_i can also be written in terms of the N electron configurations $\{\phi_i\}$. The set $\{\chi_i\}$ therefore spans some subspace of \hat{A} . We can then define the desired projector P onto this subspace as

$$P = \sum_{i=1}^n |\chi_i\rangle\langle\chi_i| \quad , \quad (3.4)$$

and the conjugate projector Q as

$$Q = 1 - P \quad . \quad (3.5)$$

What these definitions mean physically is that any element in the P subspace of \hat{A} can be written as an antisymmetric product of an ion wavefunction for $N-1$ electrons and another function $f(\vec{r}_N)$, while an element in the Q subspace cannot. That is, the bound function ϕ in the golden rule formula is an element only of the Q subspace. In fact, ϕ is an eigenfunction of $Q\hat{H}Q$,⁷ so that both ϕ and E_r can be easily determined, as we will see.

We now consider the appropriate form for the continuum function χ which we shall use in the golden rule expression, following closely the development of Miller, et al.¹³ As a physical assumption, suppose we take

$$\chi(\vec{r}_1, \dots, \vec{r}_N) = A \psi_{\text{ion}}(\vec{r}_1, \dots, \vec{r}_{N-1}) \phi_c(\vec{r}_N) \quad , \quad (3.6)$$

where ϕ_c is a coulomb orbital for the ionized electron with asymptotic energy ϵ and direction $\hat{\epsilon}$. Employing a partial wave expansion of ϕ_c about the major interparticle axis, we obtain

$$\phi_c(\vec{r}) = \sum_{\lambda m} Y_{\lambda m}^* i^\lambda \exp(i\sigma_\lambda) \phi_{\epsilon\lambda m}(\vec{r}) \quad , \quad (3.7)$$

where σ_λ is the usual coulomb phase shift and the partial coulomb orbital $\phi_{\epsilon\lambda m}$ is

$$\phi_{\epsilon\lambda m}(\vec{r}) = r^{-1} F_\lambda(-1/k, kr) Y_{\lambda m}(\hat{r}) \quad , \quad (3.8)$$

with $k = (2\epsilon)^{1/2}$. ($\hat{\epsilon}$ and \hat{r} are referred to the major interparticle axis.)

Since the radial coulomb function F_λ is normalized for large r as

$$F_\lambda(-1/k, kr) \sim \sin[kr + (1/k)\ln(2kr) + (\pi\lambda/2) + \sigma_\lambda] \quad , \quad (3.9)$$

the density of continuum states ρ is given by

$$2\pi\rho = 4/k \quad . \quad (3.10)$$

Defining $\chi_{\epsilon\lambda m}$ by Eq. (3.6) with $\phi_{\epsilon\lambda m}$ replacing ϕ_c , we substitute the expansion in Eq. (3.7) into the golden rule formula [Eq. (1.2)], and obtain the autoionization width in the direction $\hat{\epsilon}$:

$$\Gamma(\hat{\epsilon}) = \frac{4}{k} \left| \sum_{\lambda m} Y_{\lambda m}(\hat{\epsilon}) i^{-\lambda} \exp(i\sigma_\lambda) I_\lambda \right|^2 \quad , \quad (3.11)$$

where

$$I_\lambda = \langle \phi | H - E_r | \chi_{\epsilon\lambda m} \rangle \quad . \quad (3.12)$$

For a collinear case in which the excited and ionized states are of the same spatial symmetry, only the $m = 0$ term contributes to the summation in Eq. (3.11). (Other cases will be considered as they occur.) Furthermore, the magnitude ε of the energy of the ionized electron is fixed by energy conservation. That is, for a fixed nuclear geometry \vec{R} , ε is simply the vertical difference between the excited and ionized surfaces:

$$\varepsilon = V^*(R) - V_+(R) \quad . \quad (3.13)$$

Therefore, to get a total width, we need only integrate over angles:

$$\Gamma = \int d_2 \hat{\varepsilon} \Gamma(\hat{\varepsilon}) \quad . \quad (3.14)$$

Finally, substituting Eq. (3.11) for $\Gamma(\hat{\varepsilon})$ into Eq. (3.14) and performing the integration over $d_2 \hat{\varepsilon}$ trivially (since the $Y_{\ell 0}(\hat{\varepsilon})$ functions are orthonormal), we obtain

$$\Gamma = \frac{4}{k} \sum_{\ell=0}^{\infty} |I_{\ell}|^2 \quad , \quad (3.15)$$

where

$$I_{\ell} = \langle \phi | \bar{H} - E_{\vec{r}} | A \psi_{\text{ion}}(\vec{r}_1, \dots, \vec{r}_{N-1}) \phi_{\varepsilon \ell 0}(\vec{r}_N) \rangle \quad . \quad (3.16)$$

We now wish to obviate the problem of needing to calculate matrix elements containing coulomb functions, as in Eq. (3.16). From the discussion in the preceding chapter, it would seem reasonable to expand the coulomb orbital $\phi_{\varepsilon \ell 0}$ in the orbital basis $\{\phi_i\}$:

$$\phi_{\varepsilon \ell 0} \approx \sum_{i=1}^n a_i^{(\ell)} \phi_i \quad , \quad a_i^{(\ell)} = \langle \phi_i | \phi_{\varepsilon \ell 0} \rangle \quad . \quad (3.17)$$

In fact, Hickman, et al.,²¹ demonstrated with calculations on the $\text{He}(2^3S)+\text{H}$ system that for the choices of P and Q projectors presented above, the part of $\chi_{\epsilon\lambda 0}$ which is not square-integrable may be neglected in a calculation of the width. Therefore, we may approximate $\chi_{\epsilon\lambda 0}$ by

$$\chi_{\epsilon\lambda 0} \cong A \psi_{\text{ion}}(\vec{r}_1, \dots, \vec{r}_{N-1}) \left(\sum_{i=1}^n a_i^{(\lambda)} \phi_i(\vec{r}_N) \right), \quad (3.18)$$

or,

$$\chi_{\epsilon\lambda 0} \cong \sum_{i=1}^n a_i^{(\lambda)} \left[A \psi_{\text{ion}}(\vec{r}_1, \dots, \vec{r}_{N-1}) \phi_i(\vec{r}_N) \right], \quad (3.19)$$

where the quantity in square brackets is an element of the P subspace, as discussed above, and is identically one of the basis configurations ϕ_i of that subspace when a single determinant is chosen for ψ_{ion} , as has been done in our work. Thus, $\chi_{\epsilon\lambda 0}$ of Eq. (3.19) is a linear combination of elements in the P subspace:

$$\chi_{\epsilon\lambda 0} \cong \sum_P a_i^{(\lambda)} \phi_i, \quad (3.20)$$

where the P subscript signifies that ϕ_i is a member of the P subset.

Furthermore, since the bound function ϕ of Eq. (3.16) is an eigenfunction of $\hat{Q}\hat{H}\hat{Q}$, it can be written as a linear combination of elements in the Q subspace:

$$\phi = \sum_Q b_j \phi_j. \quad (3.21)$$

Using the expressions for $\chi_{\epsilon} \chi_0$ and ϕ given by Eqs. (3.20) and (3.21), we obtain:

$$I_{\lambda} = \sum_Q b_j \sum_P a_i^{(\lambda)} \langle \phi_j | H - E_r | \phi_i \rangle \quad (3.22)$$

But since ϕ_j and ϕ_i have been constructed from the same set of orthonormal orbitals, they are orthonormal, so the $-E_r$ term is zero, and we are thus left with only off-diagonal (i.e., $\hat{P}\hat{H}\hat{Q}$) matrix elements which are normally calculated in a CI procedure. Our final working equation is therefore given by

$$\Gamma = \frac{4}{k} \sum_{\lambda=0}^{\infty} \left| \sum_Q b_j \sum_P a_i^{(\lambda)} H_{ji} \right|^2 \quad (3.23)$$

Before proceeding to some actual calculations using Eq. (3.23), we will summarize the basic steps in the computation:

1. An orbital basis set $\{\phi_1^i, \dots, \phi_n^i\}$ is chosen. An orthogonal transformation is performed on them (i.e., a self-consistent-field calculation is done) to generate better orbitals $\{\phi_1, \dots, \phi_n\}$ from which we construct the $N-1$ electron ψ_{ion} function, the ground state of the core ion. This procedure also provides V_+ , the ionized state energy at the given nuclear geometry.

2. The same $\{\phi_1, \dots, \phi_n\}$ set is used to construct a set of N electron configurations needed for a CI calculation.

3. This configuration set is divided into P and Q subspaces, with the P configurations following the Q configurations. P configurations are those which have the form of $\psi_{ion} \cdot$ another orbital. All other configurations are in the Q subspace.

4. The Hamiltonian matrix \hat{H}_{ij} is computed. It has the following blocked form:

$$\left[\begin{array}{c|c} \hat{Q}\hat{H}\hat{Q} & \hat{P}\hat{H}\hat{Q} \\ \hline \hat{Q}\hat{H}\hat{P} & \hat{P}\hat{H}\hat{P} \end{array} \right] .$$

5. The $\hat{Q}\hat{H}\hat{Q}$ block of \hat{H} is diagonalized to yield ϕ (i.e., the $\{b_j\}$ coefficients) and E_r , the resonance energy V^* for the given nuclear geometry.

6. From V_+ and V^* , ϵ is computed from Eq. (3.13), giving $k = (2\epsilon)^{1/2}$. The $a_i^{(2)}$ coefficients are then obtained by evaluating the necessary overlap integrals of Eq. (3.17).

7. Finally, using the $\hat{P}\hat{H}\hat{Q}$ block of matrix elements, Eq. (3.23) is evaluated to yield the width at the given nuclear geometry.

IV. THE $\text{He}(2^3\text{S})+\text{H}_2$ SYSTEM: POTENTIAL ENERGY AND WIDTH SURFACES

The chapter presents the results for the potential energies V^* and V_+ and widths Γ for the $\text{He}(1s2s^3\text{S})+\text{H}_2$ system as functions of the nuclear geometry, obtained from the stabilization--golden rule method described in Chapter III. Because the excitation energy of $\text{He}(2^3\text{S})$ is so large (~ 20 eV), ionization must be considered for all nuclear geometries. The geometric parameters for this system are shown in Figure II. R is the distance from the helium to the midpoint of H_2 , r is the H_2 bondlength, and θ is the angle between the two.

It should be pointed out here that the only other theoretical calculation of the potentials and widths for this system were carried out by Cohen and Lane,²² who also studied the corresponding singlet system. However, their procedure is somewhat limited in applicability, as they employed a smaller, valence-bond CI with a single-center expansion to describe the H_2 molecule. In addition, they present results only for the equilibrium bond length of H_2 . They also obtained widths using a golden-rule procedure as described above, but employing a slightly different (and less practical) expansion of the coulomb orbital in L^2 functions than that used here.

The self-consistent-field and Hamiltonian matrix element calculations described in Chapter III were performed with the GAUSSIAN 70 SCF program²⁷ plus the CI package developed by Morokuma and co-workers.²³ The basis set of Slater type orbitals used in our calculations is given in Table III. Each STO in this list was expanded in six Gaussian orbitals, with exponent scaling factors recommended by Hehre, et al.²⁸ This "double zeta plus polarization" level basis set was used in

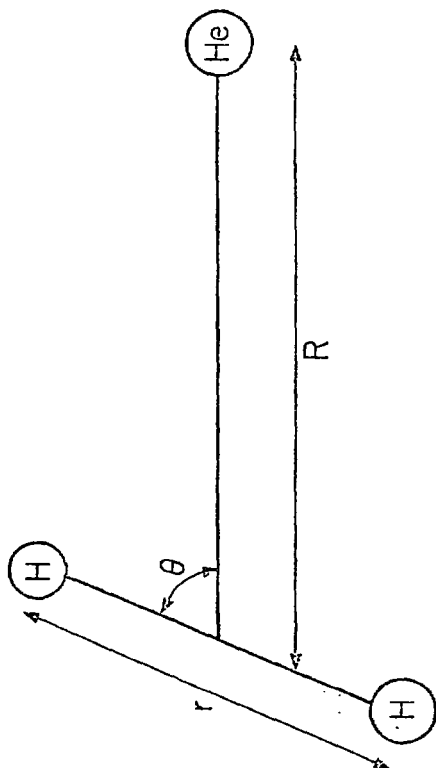
Table III. Basis set of Slater-type orbitals for the calculations on $\text{He}(2^3S)\text{-H}_2$.^a

Atom	Orbital	Zeta
He	1s	2.00
	1s	1.00
	2s	0.61
	$2p_x, 2p_y, 2p_z$	0.61
Each H	1s	1.50
	1s	1.00
	$2p_x, 2p_y, 2p_z$	1.00

^a Each STO was expanded in 6 Gaussian-type orbitals.

Figure 11. Coordinates (R, θ, r) specifying the geometry of $\text{He}+\text{H}_2$.

Figure 11.



order to accurately describe both the He^*H_2 resonance and HeH_2^+ ionic states. However, in order to be able to identify the resonant eigen-solution of $\hat{Q}\hat{H}\hat{Q}$, only a single 2s orbital was included in the basis set, with an exponent that was optimized in a separate calculation of $\text{He}(2^3\text{S})$. It was thus hoped that the resonant root could be characterized as having a major contribution from the configuration corresponding to a single excitation from the lowest molecular orbital (essentially a 1s orbital on He) to the molecular orbital most resembling a 2s orbital on He. This was found to be true. In fact, since the resonant state we are interested in has triplet spin symmetry, it was usually the lowest root of $\hat{Q}\hat{H}\hat{Q}$.

The SCF procedure described above was then used to obtain good molecular orbitals for a description of the ground state of HeH_2^+ , as required by our choices for the P and Q projectors. In order to demonstrate that this choice of molecular orbitals does not significantly harm the accuracy of the CI description of the He^*H_2 state, tests were run with different basis sets. Since it is well known that when every possible symmetry-allowed configuration arising from a given orbital set is retained in the CI basis (i.e., when a full CI is performed), the eigenvalues of the CI Hamiltonian do not change when the basis orbitals are rotated (as happens in the SCF procedure), we first considered an orbital basis set which was sufficiently small that a full CI could be performed. Such a basis was obtained by deleting the hydrogenic p orbitals from the basis given in Table III. CI potential energy and width results for this basis were then compared with those obtained from a CI calculation in which only single and double excitations from the ground state reference occupancy $\phi_1\phi_1\phi_2\phi_2$ are retained. (Again, since the ϕ_1 and ϕ_2 orbitals are obtained from an SCF calculation

of the HeH_2^+ ground state, $\psi_{\text{HeH}_2^+} = |\phi_1 \bar{\phi}_1 \phi_2|$, then ϕ_1 is essentially a He 1s orbital and ϕ_2 is essentially a 1 σ orbital for H_2^+ .) Except for the expected differences in asymptotic ($R \rightarrow \infty$) limits, the potential surfaces obtained in these calculations were virtually identical, and the width surfaces differed by less than 5%. Therefore, in our final calculations with the full orbital basis of Table III, we retained only single and double excitations in the CI wavefunction. This produced a manageable number of configurations spanning the QHQ subspace: 150 3A_1 configurations for C_{2v} ($\theta = 90^\circ$) geometries, 237 $^3\Sigma^+$ configurations for $C_{1\text{ov}}$ ($\theta = 0^\circ$), and 315 $^3A'$ configurations for C_s ($\theta = 45^\circ$). Two further tests of the potential surface were then carried out for this basis. First, with the helium far removed (i.e., $R \rightarrow \infty$), the H_2 bond length (r) was varied, and the dependence of the energy was found to be exactly that for an isolated H_2 molecule.²⁴ Second, with one of the hydrogens far removed and the other near the helium, the energy dependence was in good agreement with the $\text{He}(2^3S)+\text{H}$ results of Hickman, et al.²¹

The dimensions of the PHP blocks of the matrix, i.e., the number of P-type configurations, were relatively small: 6 for C_{2v} geometries, 8 for $C_{1\text{ov}}$, and 11 for C_s . This is fortunate in that these are the numbers of coefficients $a_i^{(\ell)} = \langle \phi_i | \phi_{\ell 0} \rangle$ which must be computed for each ℓ in the partial wave sum for Γ . The overlaps were evaluated by Gaussian quadrature, with the coulomb orbital (which is centered at the midpoint of H_2) evaluated using the continued fraction algorithm of Steed.²⁵

It is worthwhile to point out that once the QHQ block is diagonalized and the $\{b_j\}$ coefficients for the resonant root have been determined, the quantity $\sum_j b_j H_{ji}$ can be computed for each of the (6-11) i values of the P

subspace. As the CI matrix is now no longer needed, the $a_1^{(l)}$ coefficients, and the $I_{\frac{1}{2}}$ values and total Γ can then be computed in a separate calculation. Before this can be done, however, the energy of the ejected electron given in Eq. (3.13) must be computed and corrected for the errors in the asymptotic ($R \rightarrow \infty$) limits of the V^* and V_+ surfaces. The correct asymptotic limit for $\text{He} + \text{H}_2^+(r=2.0)$ of -3.5063 a.u. was taken from Edmiston, et al.²⁶ For $\text{He}(2^3\text{S}) + \text{H}_2(r=1.40)$, the correct asymptotic limit of -3.3495 a.u. was computed by adding together the energy of two hydrogen atoms (-1.0 a.u.), the experimentally accepted H_2 well depth ($D_e = 0.1743$ a.u.), the helium ground state (-2.9037 a.u.), and the excitation energy of the $1s2s^3\text{S}$ state (0.7284 a.u.).

One final comment must be made concerning our calculations. Even though this is a triatomic system, only $m = 0$ contributions were included in the partial wave summation for Γ (see Eq. (3.11) and the subsequent discussion). This procedure is valid for the following reasons: For $C_{\infty v}$ (collinear) geometries the ionization is a $\Sigma \rightarrow \Sigma$ transition, so only the $m = 0$ term contributes, as discussed in Chapter III. For C_{2v} (perpendicular) geometries, only even m terms can contribute, since the R axis is also an axis of C_2 symmetry. Also, the maximum l (and hence m) in the orbital basis of Table III is $l = 1$, so that only the $m = 0$ term will contribute in this case; otherwise, the angular integrations in $I_{\frac{1}{2}}$ [see Eq. (3.12)] involving the product of ϕ and the coulomb orbital will give zero. Finally, in the C_s ($\theta = 45^\circ$) case, all m contribute in principle, so that the $m = 1$ term does have a non-zero effect in this case. However, this contribution has been shown to be small,²² as the resonant wavefunction ϕ contains only very small contributions from configurations which do not possess Σ symmetry. This implies that the

H₂ may be treated as a nearly spherically symmetric entity, an argument which is borne out by the fact that V* and Γ are fairly insensitive to the angle θ, and that these quantities change smoothly as θ is varied from 0° to 90°. An additional fact which supports this argument is that if the H₂ is treated as spherically symmetric, calculated ionization cross sections for various collision energies are in excellent agreement with those calculated by treating the H₂ as a rigid rotator (see Chapter V). It was thus felt that m = 1 terms could be neglected in these calculations.

Potential energies V* and V₊ and widths Γ were calculated for several values of R, θ, and r (cf. Figure II). (The nuclear repulsion energy is always included in the potentials.) The complete results are listed in Table IV. Even though the orbital basis set was not optimized for the HeH₂⁺ system, the collinear SCF V₊ energies we obtained are in good agreement with the results of Brown and Hayes.²⁹ In addition, the V* results we obtained are in good agreement with, though somewhat less repulsive for R < 6 a₀, than those obtained by Haberland³⁰ by fitting molecular beam differential cross section measurements.

Since there are three degrees of freedom in this system, it is difficult to graphically display the results. However, as the scattering calculations presented elsewhere in this thesis are based on a rigid rotator approximation to the H₂ molecule (see Chapter V), we will discuss the "slices" of the excited state V* potential and width Γ corresponding to a fixed value of r = 1.40 a₀ (the equilibrium bond length). Such slices of V* and Γ are shown in Figures III and IV, respectively. Considering Figure III, we see that the potential is basically repulsive, as would be expected from the repulsion of the excited helium electron

Table IV. Results for V^* , V_+ , and Γ for HeH_2^a .

R	G	r ^b	V^*	Γ	V_+
3.0	0	1.00	-3.186143	6.06×10^{-3}	-3.309554
3.0	0	1.25	-3.216686	3.78×10^{-3}	-3.396816
3.0	0	1.30	-3.216311	3.47×10^{-3}	-3.407380
3.0	0	1.35	-3.214490	3.19×10^{-3}	-3.416385
3.0	0	1.40	-3.211431	2.95×10^{-3}	-3.424050
3.0	0	1.80	-3.158920	1.52×10^{-3}	-3.454388
3.0	45	1.40			-3.421032
3.0	90	1.00	-3.208059	7.34×10^{-3}	-3.304738
3.0	90	1.35	-3.255670	4.31×10^{-3}	-3.410330
3.0	90	1.40	-3.255828	4.03×10^{-3}	-3.417774
3.0	90	1.45	-3.255040	3.79×10^{-3}	-3.424046
3.0	90	1.80	-3.233047	2.60×10^{-3}	-3.445639
4.0	0	1.00	-3.240024	2.96×10^{-3}	-3.306871
4.0	0	1.30	-3.282371	1.98×10^{-3}	-3.405918
4.0	0	1.35	-3.282938	1.88×10^{-3}	-3.415042
4.0	0	1.40	-3.282363	1.80×10^{-3}	-3.422804
4.0	0	1.45	-3.280818	1.73×10^{-3}	-3.429387
4.0	0	1.80	-3.252833	1.48×10^{-3}	-3.453140
4.0	0	3.00	-3.175245		-3.436948
4.0	45	1.40	-3.289316	1.71×10^{-3}	-3.422144
4.0	90	1.00	-3.246569	2.83×10^{-3}	-3.305512
4.0	90	1.35	-3.294546	1.56×10^{-3}	-3.413793
4.0	90	1.40	-3.294770	1.40×10^{-3}	-3.421556

Table IV, continued.

R	θ	r	v^2	τ	v_4
4.0	90	1.45	-3.294643	1.35×10^{-3}	-3.428131
4.0	90	1.80	-3.272238	8.69×10^{-4}	-3.451656
5.0	0	1.40	-3.296840	4.23×10^{-4}	-3.421461
5.0	0	2.50	-3.222522	6.14×10^{-4}	-3.447638
5.0	0	3.00	-3.214261		-3.433381
5.0	0	4.00	-3.201510		-3.404606
5.0	45	1.40	-3.299139	3.67×10^{-4}	-3.421413
5.0	90	1.40	-3.300987	2.88×10^{-4}	-3.421385
6.0	0	1.00	-3.254250	9.15×10^{-5}	-3.305166
6.0	0	1.35	-3.301680	7.07×10^{-5}	-3.413280
6.0	0	1.40	-3.301857	6.96×10^{-5}	-3.420990
6.0	0	1.45	-3.301094	6.88×10^{-5}	-3.427517
6.0	0	1.80	-3.279458	6.91×10^{-5}	-3.450831
6.0	0	4.0	-3.200593		-3.403446
6.0	45	1.40	-3.302615	6.01×10^{-5}	-3.420994
6.0	90	1.00	-3.255096	8.10×10^{-5}	-3.304798
6.0	90	1.40	-3.303270	4.89×10^{-5}	-3.421038
6.0	90	1.80	-3.280749	3.66×10^{-5}	-3.451174
6.5	0	7.0	-3.202478		-3.370072
7.0	0	1.40	-3.304333	1.05×10^{-5}	-3.420802
7.0	45	1.40	-3.304538	8.97×10^{-6}	-3.420765
7.0	90	1.40	-3.304747	7.58×10^{-6}	-3.420827
7.5	0	7.0	-3.191493		-3.363930
8.0	0	1.00	-3.257331	1.57×10^{-6}	-3.304754
8.0	0	1.35	-3.305258	1.58×10^{-6}	-3.413002
8.0	0	1.40	-3.305482	1.62×10^{-6}	-3.420712

Table IV, continued.

R	θ	r	V^a	V^+	V_+
8.0	0	1.45	-3.364759	1.66×10^{-6}	-3.427236
8.0	0	1.60	-3.283062	2.00×10^{-6}	-3.450479
8.0	45	1.45	-3.305513	1.32×10^{-6}	-3.420696
8.0	90	1.00	-3.257388	1.26×10^{-6}	-3.304600
8.0	90	1.40	-3.305565	1.10×10^{-6}	-3.420713
8.0	90	1.80	-3.282984	1.16×10^{-6}	-3.450615
9.0	0	1.40	-3.305947	2.46×10^{-7}	-3.420662
9.0	90	1.40	-3.305940	1.50×10^{-7}	-3.420653
10.0	0	1.40	-3.306108	3.82×10^{-8}	-3.420630
10.0	45	1.40	-3.306093	2.65×10^{-8}	-3.420622
10.0	90	1.40	-3.306087	1.89×10^{-8}	-3.420620
14.5	0	23.0	-3.206108		-3.368466
15.0	0	22.0	-3.200393		-3.360546
17.0	0	18.0	-3.134897		-3.358469
19.5	0	13.0	-3.129821		-3.358542
23.0	0	6.0	-3.129245		-3.369969
24.5	0	3.0	-3.160897		-3.431992
25.0	0	1.40	-3.306141		-3.420572
25.0	90	2.00			-3.453147
25.0	90	1.00	-3.257929		-3.304509
25.0	90	1.35	-3.305916		-3.412854
25.0	90	1.40	-3.306141		-3.420572
25.0	90	1.45	-3.305415		-3.427102
25.0	90	1.80	-3.283589		-3.450367

^a The energies for HeH_2^+ were determined from the SCF wave function. The exact asymptotic limits for these potentials are $V^+(R \rightarrow \infty, r = 1.4) = -3.3495$ a.u. and $V_+(R \rightarrow \infty, r = 2.0) = -3.5063$ a.u.

^b R , r , and θ are the coordinates defined in Figure II.

from the closed shell H_2 . The long-range van der Waals attraction was not calculated, since it would not have been reliable for our choice of basis set. We also see that the potential is not very anisotropic, justifying the concept of a spherically symmetric H_2 discussed above. From Figure IV, we note that although there is some leveling off for small R , Γ shows the typical exponential behavior calculated or estimated for other autoionizing molecules. This is not surprising, since in the golden rule picture, Γ depends on the overlap of two functions which are exponentially decaying in R .

For the scattering calculations presented in the following chapter, it is quite useful to parameterize the potential V^* with width Γ for fixed r by the following Legendre expansions:

$$V^*(R, \theta) = \sum_{\ell=0}^{\infty} v_{\ell}(R) P_{\ell}(\cos\theta) \quad , \quad (4.1)$$

$$\Gamma(R, \theta) = \sum_{\ell=0}^{\infty} \Gamma_{\ell}(R) P_{\ell}(\cos\theta) \quad , \quad (4.2)$$

where, since H_2 is homonuclear, only even terms contribute. Since the potential and width are fairly isotropic, these expansions should converge rapidly. In fact, since V^* and Γ were calculated for three values of θ at each R , we have assumed that the series can be truncated after the first three terms ($\ell = 0, 2, 4$). That is, we substitute results (at each R) for $\theta = 0^\circ, 45^\circ$, and 90° into Eqs. (4.1) and (4.2) and solve explicitly for the Legendre moments v_{ℓ} and Γ_{ℓ} :

$$v_0(R) = \frac{1}{15} [V(R, 0^\circ) + 8 \cdot V(R, 45^\circ) + 6 \cdot V(R, 90^\circ)] \quad , \quad (4.3)$$

Figure III. Interaction potential $V^*(R, \theta)$ for $\text{He}(2^3\text{S})+\text{H}_2$ with θ fixed at $0^\circ(\text{C}_{\infty\text{v}})$, $45^\circ(\text{C}_s)$, and $90^\circ(\text{C}_{2\text{v}})$. The H_2 bond length is fixed at the equilibrium value $r_0 = 1.40 \text{ a}_0$. The calculated asymptotic limit for this potential is $V^*(R \rightarrow \infty, r = 1.40) = -3.306141 \text{ a.u.}$

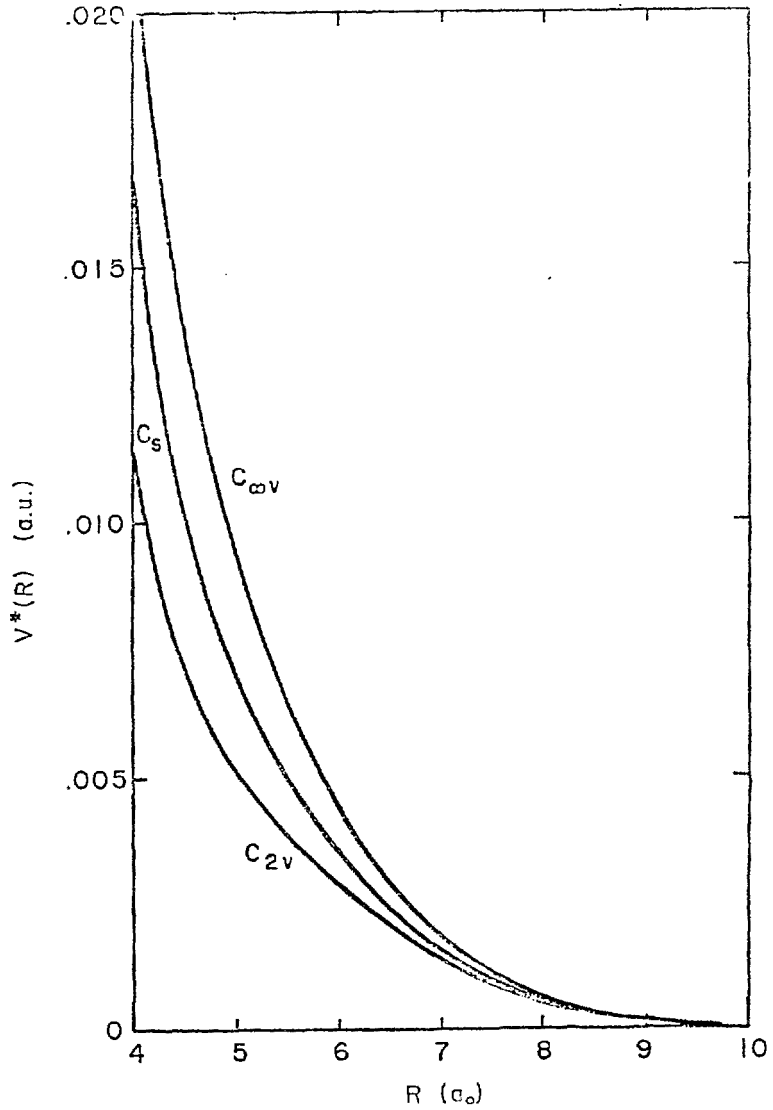
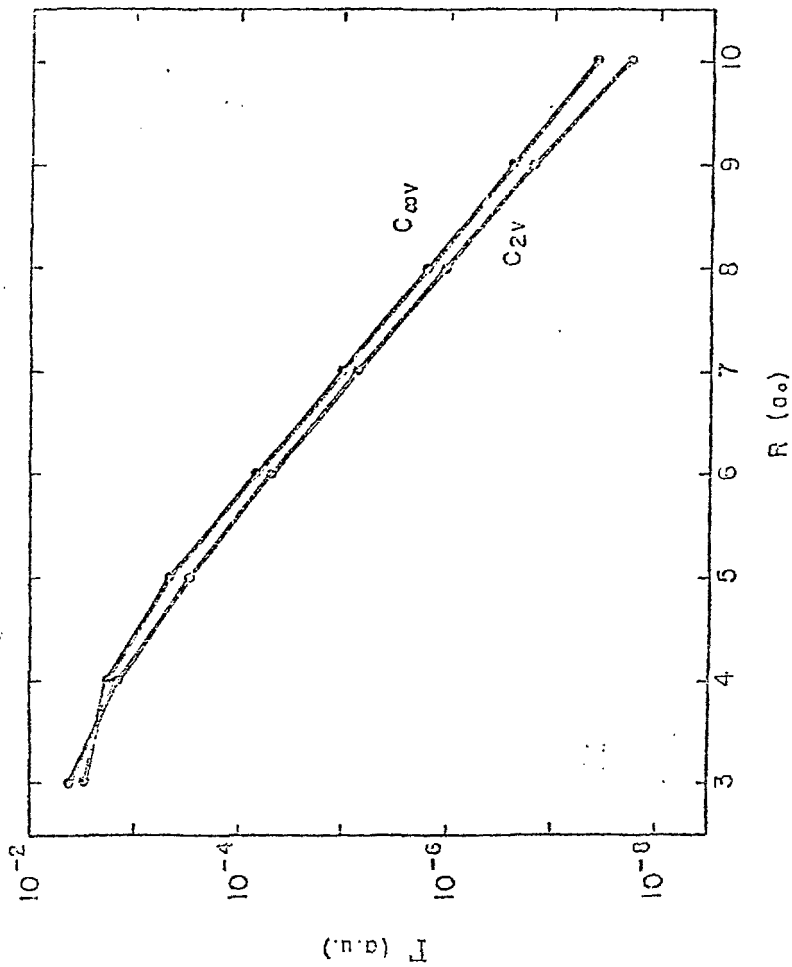


Figure IV. Autoionization width $\Gamma(R, \theta)$ for $\text{He}(2^3\text{S})\text{H}_2$ with θ fixed at 0° ($C_{\infty v}$) and 90° (C_{2v}). The H_2 bond length is fixed at the equilibrium value $r_0 = 1.40 \text{ a}_0$. The $\theta = 45^\circ$ (C_s) results lie in between those of $\theta = 0^\circ$ and $\theta = 90^\circ$, and have been omitted for clarity.

Figure IV.



$$v_2(R) = \frac{2}{21} [5 \cdot V(R, 0^\circ) + 4 \cdot V(R, 45^\circ) - 9 \cdot V(R, 90^\circ)] \quad , \quad (4.4)$$

$$v_4(R) = \frac{16}{35} [V(R, 0^\circ) - 2 \cdot V(R, 45^\circ) + V(R, 90^\circ)] \quad , \quad (4.5)$$

with analogous equations for Γ_0 , Γ_2 , and Γ_4 . These Legendre moments for V^* and Γ are tabulated in Table V and are plotted in Figures V and VI, respectively. Since $v_0 > v_2 \gg v_4$, this procedure appears justified. In fact, Γ_4 is so small relative to Γ_2 that it can be neglected.

Considering briefly the r dependence of the potential and width surfaces, we found that for $R \geq 6 a_0$, the equilibrium value of r (r_0) is unchanged from the value for an isolated H_2 molecule. In fact, even at $R = 3 a_0$, r_0 is only $0.12 a_0$ less than the isolated value. Furthermore, a cubic fit of the potential in r about r_0 (for fixed R and θ) of the form

$$V^*(r) = V^*(r_0) + \alpha(r-r_0)^2 + \beta(r-r_0)^3 \quad (4.6)$$

shows that in the $C_{\infty v}$ case, the α and β coefficients at $R = 3 a_0$ only change by 52% and 12%, respectively, from their asymptotic values; for the C_{2v} case, α and β remain virtually unchanged at $R = 3 a_0$. These facts strongly suggest that the electronic structure of the H_2 is relatively unperturbed until $R \leq 3 a_0$. Since at thermal energies the region $R < 5 a_0$ is roughly energetically forbidden (cf. Figure V), and since the dependence of Γ on r was not found to be pronounced for r near r_0 , treating the H_2 as a rigid rotator in the calculations of ionization cross sections seems a reasonable approximation. Such calculations are presented in the following chapter.

Table V. Legendre expansion coefficients of the potential energy surface and width, in atomic units.

$R(a_0)$	v_0	v_2	v_4	Γ_0	Γ_2
3	.065113	.029598		3.67×10^{-3}	7.20×10^{-4}
4	.015107	.007986	.000685	1.59×10^{-3}	3.09×10^{-4}
5	.006416	.002679	.000206	3.39×10^{-4}	9.44×10^{-5}
6	.003315	.000922	.000047	5.62×10^{-5}	1.41×10^{-5}
7	.001533	.000277	-.000002	8.52×10^{-6}	1.92×10^{-6}
8	.000609	.000059	-.000010	1.25×10^{-6}	3.31×10^{-7}
9	.000199	-.000005		1.82×10^{-7}	6.40×10^{-8}
10	.000049	-.000012	-.000004	2.42×10^{-8}	1.21×10^{-8}

Figure V. Legendre moments $v_\lambda(R)$, $\lambda = 0, 2, 4$, of the $\text{He}(2^3\text{S})+\text{H}_2$ potential energy surface [cf. Eq. (4.1)]. The H_2 bond length is fixed at the equilibrium value $r_0 = 1.40 a_0$.

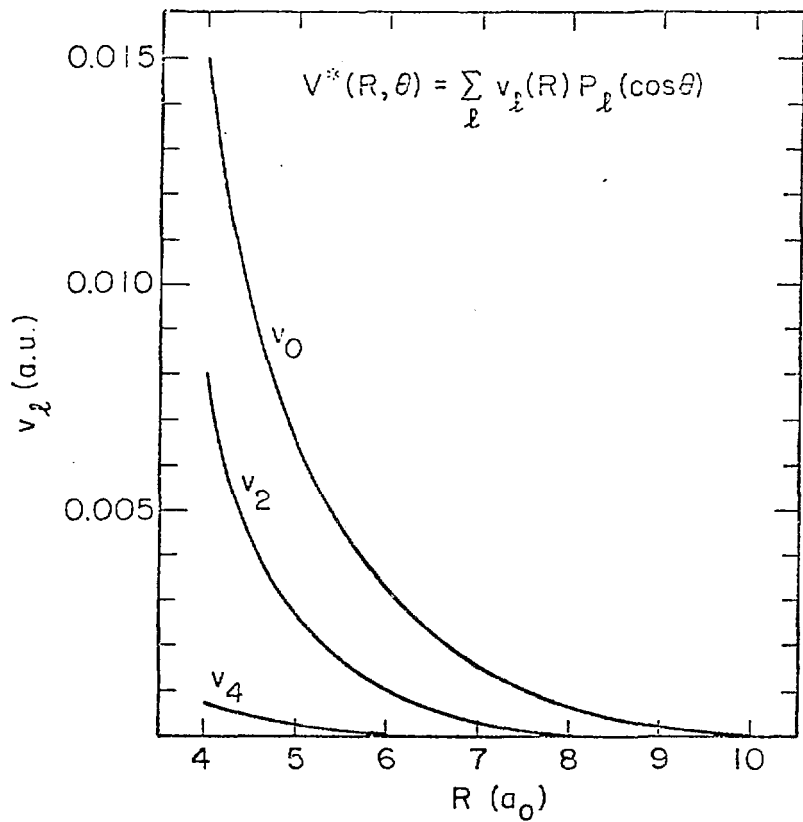
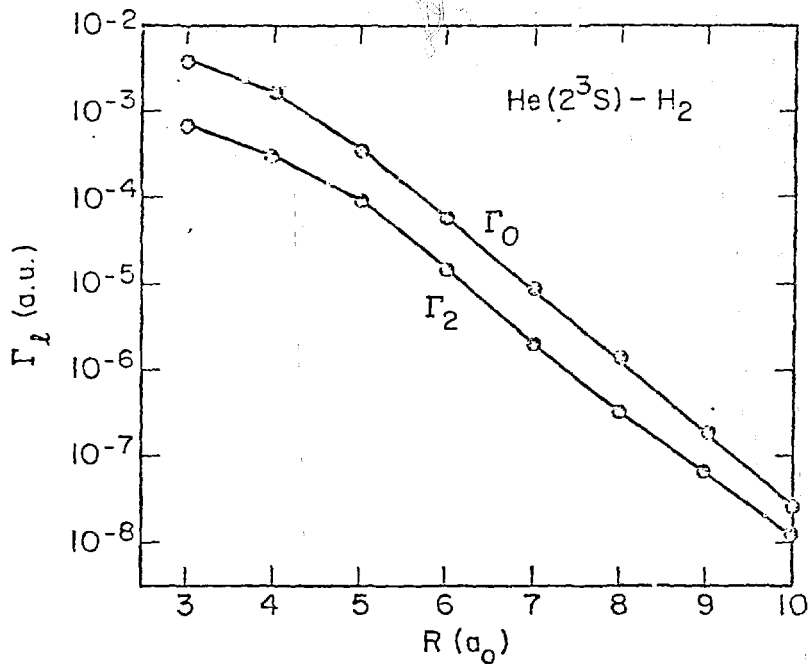
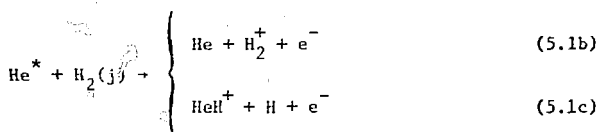


Figure VI. Legendre moments $\bar{\Gamma}_\lambda(R)$, $\lambda = 0, 2$, of autoionization width for $\text{He}(2^3\text{S})+\text{H}_2$ [cf. Eq. (4.2)]. The H_2 bond length is fixed at the equilibrium value $r_0 = 1.40 a_0$.



V. SCATTERING CALCULATIONS ON THE $\text{He}(2^3\text{S})+\text{H}_2$ SYSTEM

This chapter presents a study of the scattering of triplet metastable helium, $\text{He}(2^3\text{S})$, by an H_2 molecule. Such a study is worthwhile for a number of reasons. First, several elastic and reactive channels are possible:



Second, because the system has only four electrons, extensive CI calculations for the interaction potentials and autoionizing width are feasible. In fact, such calculations have already been presented for this system in the previous chapter. Third, as was discussed above, the interaction potential V^* between He^* and H_2 is basically repulsive, so the cross sections for the various reactions given in Eq. (5.1) should be strongly energy dependent. This means that the accuracy of the calculated cross sections should provide a sensitive test of the potential and width. Finally, it is possible to judge the accuracy of our cross sections, as there is a considerable amount of experimental data³¹⁻³⁵ with which to compare.

The potentials and widths presented in the last chapter have been used in both quantum mechanical and classical studies of the cross sections for the reactions given in Eq. (5.1). In Section A, we discuss

quantum mechanical close-coupling calculations of the elastic, rotationally inelastic, and total ionization cross sections in the (center-of-mass) collision energy range 0.010 to 0.500 eV.³⁶ Section B presents a discussion of classical calculations of the total ionization and associative ionization cross sections, based on a spherically symmetric approximation to the H₂ molecule, in the energy range 0.010 to 1.000 eV.

A. Quantum Mechanical Calculations

In this section, we discuss quantum mechanical close-coupling calculations of the various cross sections related to the scattering of He(2³S) by H₂,³⁶ based on a rigid rotator approximation to the H₂. The CI interaction potential and autoionization widths needed for these calculations were presented in Chapter IV. A brief summary of the theoretical aspects of the calculations is given in Section I. Cross section and total ionization rate constants are presented in Section 2, and are shown to be in good agreement with the experimental results of Lindinger, *et al.*³⁷

1. Theoretical Considerations

The scattering calculations presented in this section are based on the well-known Arthurs and Dalgarno formalism for the scattering of an atom by a rigid rotator,³⁸ and are exact within this approximation. For the present case in which ionization is possible, however, the loss of incident He* atoms due to Penning ionization is described by the complex potential,^{18,39-42} $(V^* - \frac{1}{2}\Gamma) \equiv V$, where V* is the interaction potential for He(2³S)+H₂ and Γ is the autoionization width. Roughly speaking, since the square modulus of the true wavefunction is proportional to

$$|\exp[-i(V^* - \frac{i}{2}\Gamma)\tau/\hbar]|_i^2 = \exp(-\Gamma\tau/\hbar) \quad , \quad (5.2)$$

we see that the width corresponds to a damping of the resonant state, i.e., a loss of the excited specie to ionization. The inclusion of this imaginary part of the potential is the only change needed in the Arthurs and Dalgarno formalism. The coupled-channel equations arising from the complex, angularly-dependent potential $V^* - \frac{i}{2}\Gamma$ are then numerically integrated to provide the complex S-matrix, from which the various cross sections can be derived. Since the method employed here and tests of its accuracy are presented elsewhere⁴³ (see also Ref. 36 and references contained therein), we will present only a brief summary of the theory and computational method.

We start by considering the Schrödinger equation for our problem

$$(H_0 + H_1 - E)\Psi = 0 \quad , \quad (5.3)$$

where $H_0 = H_0(R)$ is only a function of the radial distance (cf. Figure II) and $H_1 = H_1(R, \theta)$ is a function of both radial distance and angular orientation. (In terms of a Legendre expansion of $(V^* - \frac{i}{2}\Gamma) \equiv V$ as in Eqs. (4.1) and (4.2), H_0 contains the $\ell = 0$ term of this expansion [$V_0(R)$] while the higher order terms comprise H_1 [$V_2(R)$, $V_4(R)$, etc.] .) We next express the approximate set of solutions to Eq. (5.3) as

$$\Psi_{JM} = \sum_{n=1}^N \frac{1}{R} U_{j_n \ell_n JM}(R) y_{j_n \ell_n JM}(\hat{R}, \hat{r}) \quad , \quad (5.4)$$

where J is total angular momentum quantum number, $j(\ell)$ is the rotational (orbital) angular momentum quantum number, and y is related to the product

of spherical harmonics $Y_{j m_j}(\hat{R}) Y_{l m_l}(\hat{r})$ by a Clebsch-Gordan series. The solutions Ψ_{JM} are approximate since the summation is finite. Using Eq. (5.4) in Eq. (5.3) leads to a set of N coupled-channel equations (expressed in matrix notation):

$$(\underline{H}_0 + \underline{H}_1) \cdot \underline{U} = 0 \quad , \quad (5.5)$$

where the elements of \underline{H}_0 are given by

$$(\underline{H}_0)_{nn'} = \delta_{nn'} \left\{ \frac{d^2}{dR^2} + k^2 - \frac{2mj}{2I} \frac{(j+1)}{n} - V_0(R) - \frac{l(l+1)}{R^2} \right\} \quad , \quad (5.6)$$

and where the elements of \underline{H}_1 involve products of $V_l(R)$ times angular integrals of $P_l(\cos\theta)$ with the y functions. The solutions $\underline{U}^{(i)}$ to Eq. (5.5) are expressed in terms of the components $U_{j', l}^{j, l}(R)$, where $U_{j', l}^{j, l}$ is the amplitude for a transition between the approximate states $j'l$ and $j'l'$. Since the $V_l(R)$ functions are complex, the coupled channel equations of Eq. (5.5) have complex solutions. These solutions can be generated using a complex version of the Numerov algorithm.⁴⁴ In this procedure, the N complex coupled-channel equations are separated to give $2N$ real coupled equations, to which we determine N linearly independent complex regular solutions $\underline{Y}^{(i)}$. The proper linear combinations of these $\underline{Y}^{(i)}$ must then be taken to insure that our solutions have the correct asymptotic behavior. To accomplish this, the asymptotic form of our complex solutions is matched direction to the complex S -matrix. Following the notation of Arthurs and Dalgarno,³⁸ we write the desired asymptotic form as

$$U_{j, \ell}^{j, \ell}(R) \sim \delta_{jj'} \delta_{\ell\ell'} \exp[-i(k_j R - \frac{2\pi}{2})] - (\frac{k_j}{k_j'})^{1/2} S^J(j', \ell', j, \ell) \cdot \exp[i(k_j R - \frac{2\pi}{2})] \quad (5.7)$$

For convenience, we write Eq. (5.7) in matrix notation, so that for each J , we have $N \times N$ complex matrices

$$\underline{U}^J = \underline{H}^- - \underline{H}^+ \cdot \underline{K}^{-1/2} \cdot \underline{S}^J \cdot \underline{K}^{1/2} \quad , \quad (5.8)$$

where

$$(\underline{H}^\pm)_{j, \ell', j, \ell} = \delta_{jj'} \delta_{\ell\ell'} k_j R [n_\ell(k_j R) \pm i j_\ell(k_j R)] \quad (5.9)$$

and

$$(\underline{K})_{j, \ell', j, \ell} = \delta_{jj'} \delta_{\ell\ell'} k_j \quad . \quad (5.10)$$

The j_ℓ and n_ℓ in Eq. (5.9) are spherical Bessel functions, and have asymptotic forms such that

$$[n_\ell(k_j R) \pm i j_\ell(k_j R)] \sim \frac{1}{k_j R} \exp[\pm i(k_j R - \frac{\pi\ell}{2})] \quad , \quad (5.11)$$

as is required for Eq. (5.7). Writing the set of linearly independent solutions $\underline{Y}^{(\pm)}$ as \underline{Y}^J , the asymptotic matching of Eq. (5.8) is accomplished by solving the equations

$$\underline{H}_1^- \cdot \underline{A} + \underline{H}_1^+ \cdot \underline{B} = \underline{Y}_1^J \quad (5.12)$$

$$\underline{H}_2^- \cdot \underline{A} + \underline{H}_2^+ \cdot \underline{B} = \underline{Y}_2^J \quad , \quad (5.12b)$$

where the subscripts 1 and 2 indicate that the matrices are evaluated at two large values of R , R_1 and R_2 . It can then be shown⁴³ that the S-matrix is given by

$$\underline{S}^J = -\underline{K}^{1/2} \cdot \underline{B} \cdot \underline{A}^{-1} \cdot \underline{K}^{-1/2} \quad (5.13)$$

In actual computations, the real and imaginary parts of the above matrix equations are separated for convenience.

Now that the S-matrix has been determined, the elastic and rotationally inelastic cross sections can be expressed in terms of it, exactly as Arthurs and Dalgarno have done. The ionization cross section, on the other hand, is obtained by inverting the normal proof of the unitarity of the S-matrix⁴⁵ based on the assumption of flux conservation. For the rotator initially in state j and for an initial translational energy of $E = k_j^2/2$, the total ionization cross section is then given by⁴³

$$\sigma_{\text{ion}}(j) = \frac{\pi}{(2j+1)k_j^2} \sum_{J=0}^{\infty} \sum_{\ell=|J-j|}^{J+j} (2J+1) \left[1 - \sum_{j'\ell'} |S^J(j'\ell', j\ell)|^2 \right] \quad (5.14)$$

The lack of unitarity of the S-matrix implies that the term in square brackets is non-zero, hence describing a loss of incident flux to ionization. Note that the cross section $\sigma_{\text{ion}}(j)$ given by Eq. (5.14) is for the total amount of ionization over all possible channels [e.g., for Eq. (5.1b) through (5.1d)]. Other cross sections can also be obtained from the (complex) S-matrix by application of the appropriate formulae. In particular, the differential elastic scattering cross section (i.e., the

cross section for scattered $\text{He}(2^3\text{S})$ as a function of angle with the H_2 remaining in the $j = 0$ state) is given by⁴⁶

$$\frac{d\sigma_{00}}{d\Omega} = \left| \frac{1}{2ik_0} \sum_{J=0}^{\infty} (2J+1) (S_{00}^J - 1) P_J(\cos\theta) \right|^2, \quad (5.15)$$

where S_{00}^J is the (1,1) element of the S-matrix.

2. Results

The coordinates for the $\text{He}(2^3\text{S})+\text{H}_2$ system are shown in Figure II. The complex potential $V^* - \frac{i}{2} \Gamma$ used in the calculations presented in this section was given in the preceding chapter. As discussed there, we are considering the "slice" of the V^* and Γ surfaces corresponding to a fixed H_2 bond length of $r_0 = 1.40 a_0$. We have already shown that these "slices" can be accurately expressed as a low-order sum of even order Legendre moments

$$V^* - \frac{i}{2} \Gamma = \sum_{\lambda} [v_{\lambda}(R) - \frac{i}{2} \Gamma_{\lambda}(R)] P_{\lambda}(\cos\theta) \quad (5.16)$$

Values for v_0 , v_2 , v_4 , Γ_0 , and Γ_2 are listed in Table V, and these functions are plotted in Figures V and VI. Γ_4 was found to be negligible. These moments were in turn fit to some form which can easily be interpolated. In the region spanned by the calculated values, v_0 , v_2 , and Γ_0 were fit by a cubic spline procedure. v_0 and v_2 were set to zero for $R \geq 11 a_0$ and $9 a_0$, respectively. For $R \geq 9 a_0$, Γ_0 was set to $(14.008) \exp(-2.0177 R)$ a.u., obtained by fitting the exponential form to the calculated values at $R = 9 a_0$ and $R = 10 a_0$. Finally, for all R , Γ_2 was set to $(0.73648) \exp(-1.7924 R)$ a.u. and v_4 was set to

$(0.08375) \exp(-1.2015 R)$ a.u. These approximate fits to v_4 and Γ_2 were found to be sufficiently accurate, since the total ionization cross section was insensitive to their inclusion over the entire (center-of-mass) collision energy range investigated (0.010 eV to 0.500 eV). In fact, v_4 had only a minor effect on the rotational excitation cross sections.

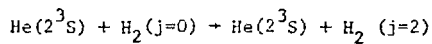
All calculations presented here were run with the OPCHANX program.⁴³ Only open (energetically allowed) rotational channels were included in our calculations. We found that including only the $j = 0$ and $j = 2$ rotational states produced converged ionization cross sections for the entire energy range studied. For example, just above the threshold for the $j = 0$ to $j = 2$ transition, inclusion of the just-opened channel produced less than a 2% variation in $\sigma_{\text{ion}}(0)$. As could be expected, the cross sections for rotational excitation were somewhat more sensitive to the addition of extra channels. For collision energies just above the $j = 0$ to $j = 4$ transition, for example, inclusion of the $j = 4$ channel increased the $\sigma_{0 \rightarrow 2}$ value by 12%.

Calculated total ionization cross sections as a function of center-of-mass collision energy are given in Table VI for the case in which the H_2 molecule is initially in the $j = 0$ state. Deviations from these results of only a few percent are obtained with the H_2 initially in the $j = 1$ or $j = 2$ states. As is apparent from Table VI, σ_{ion} is a strongly increasing function of the collision energy. This is a reflection of the fact that since V^* is repulsive, high collision energies lead (on the average) to closer approaches of the particles. But since Γ increases rapidly as R decreases, closer approaches have much higher ionization probabilities.

Table VI. Total ionization cross sections as a function of energy for
 $\text{He}(2^3\text{S})-\text{H}_2$

$E(\text{eV})$	$\sigma_i(\text{a}_0^2)$
0.010	.34
0.040	1.6
0.070	3.5
0.100	6.4
0.140	11.
0.200	20.
0.300	30.
0.400	35.
0.500	39.

Table VII. Cross sections for the rotationally inelastic process



$E(\text{eV})$	$\sigma_{0 \rightarrow 2} \text{ (a}_0^2\text{)}$
0.070	0.10
0.100	0.63
0.140	2.2
0.200	5.3

Rotational excitation cross section results for the $j = 0$ to $j = 2$ transition as a function of collision energy are given in Table VII. As in the case with σ_{ion} , σ_{0+2} also increases sharply with energy, and an analogous argument can be made for this behavior. That is, higher collision energies lead to closer approaches, where v_2 is larger. Since v_2 (and higher Legendre moments) couple the $j = 0$ and $j = 2$ states, there is consequently more rotational excitation. However, the σ_{0+2} values are much lower than those for σ_{ion} . This is due not only to the fact that Γ_0 and v_2 are of the same order of magnitude for close approaches, but also to the fact that, unlike rotational excitation, in which flux can go back and forth, ionization is a virtually irreversible process.

Assuming that both the initial and final rotational states of H_2 are $j = 0$, the angular distribution of $\text{He}(2^3\text{S})$ in elastic collisions was calculated from Eq. (5.15) at 0.100 eV. The results are shown in Figure VII with the width included (lower curve) and not included (upper curve). Two comments concerning these results are in order:

(1) The effect of including Γ is to decrease the amount of wide angle elastic scattering. Since collisions involving small impact parameters generally lead to large scattering angles for repulsive potentials, this suggests that the ionization is occurring for small impact parameters, i.e., for close approaches of the particles, as was postulated above.

(2) Unlike the total ionization cross section, the differential elastic cross section is quite insensitive to the inclusion of v_2 , as well as to the inclusion of Γ_2 . In fact, excluding both v_2 and Γ_2 causes noticeable differences only at large angles; even then, the

differences are less than 5%.

Assuming a Maxwellian distribution of collision energies, cross section results $\sigma_{\text{ion}}(E)$ can be thermally averaged to yield the ionization rate constant $k(T)$:

$$k(T) = \sqrt{\frac{3kT}{\pi m}} \int_0^{\infty} d(E/kT) (E/kT) e^{-(E/kT)} \sigma_{\text{ion}}(E) \quad , \quad (5.17)$$

where k on the right hand side of Eq. (5.17) is the Boltzmann constant. In our calculations, the integral in Eq. (5.17) was performed numerically with the trapezoid rule. The results we obtained for $k(T)$ agree reasonably well with the experimental results of Lindinger, *et al.*,³⁷ as shown in Figure VIII. Although the strong temperature dependence is correctly reproduced, our absolute values are somewhat low. In fact, if our results were scaled up by a constant factor of 1.7, they would lie well within the allowed error bars from 300° to 900°.

In general, then, the results presented in this section indicate that the V^* and Γ functions presented in Chapter IV are reasonably accurate, though not perfect in all respects. As the width is based on a golden rule expression employing an approximate continuum function (see Chapter IV), Γ could be too small, leading to ionization cross sections which are too small. This would also be the case if V^* is too repulsive (see discussion above on $\sigma_{\text{ion}}(E)$ results), but this is contraindicated by a comparison with results obtained by Haberland³⁰ by fitting his experimental differential cross sections (see Chapter IV). Some error could also be due to the approximation of H_2 as a rigid rotator, but it was felt that these errors would not be on the order of those presented here. The best way to solve the question of

Figure VII. Differential elastic scattering cross sections for $\text{He}(2^3\text{S})+\text{H}_2$ at (c.m.) collision energy $E = 0.100$ eV, assuming the initial and final rotational states of H_2 are $j = 0$. The upper curve was calculated with V^* alone, while the lower curve was calculated with $V^* - \frac{i}{2}\Gamma$. The cusp at $\theta = 20^\circ$ is due to the change in horizontal scale.

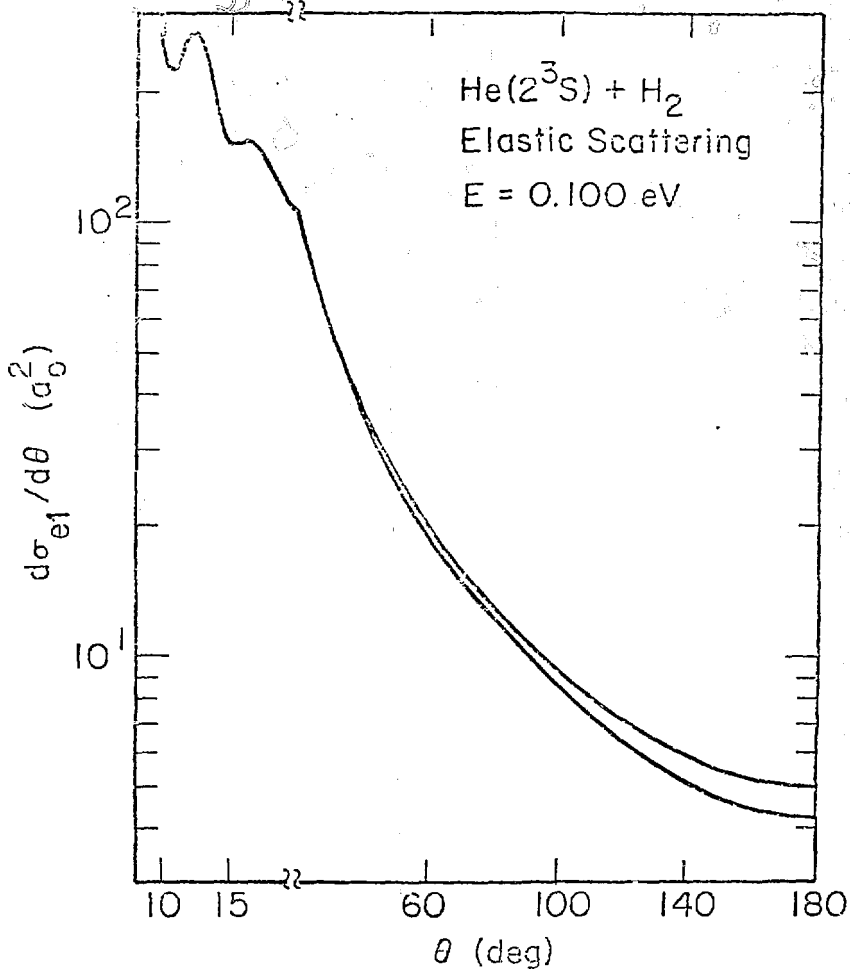
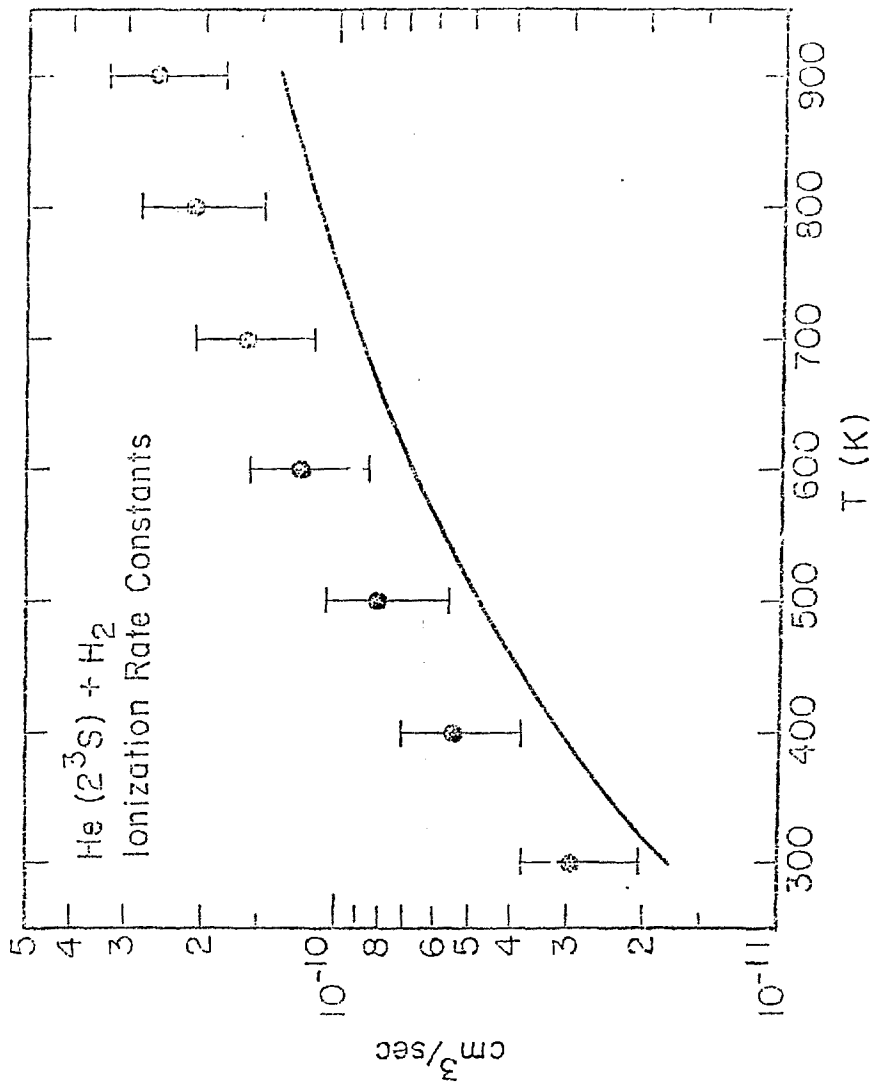


Figure VIII. Rate constants $k(T)$ for the ionization of H_2 by $He(L^3S)$ [cf. Eq. (3.17)]. The present ab initio results (solid curve) are compared with the experimental results of Lindinger, et al.³⁷



where the error lies may be by recomputing V^* and Γ by another procedure. In Chapter VIII, we discuss how a calculation of the Siegert eigenvalues for a system can provide these quantities. In fact, results for the $\text{He}(2^1, 3^3)+\text{H}$ systems indicate that the golden rule method may somewhat underestimate the width in certain cases.

B. Classical Calculations

This section presents classical calculations of the total ionization and associative ionization cross sections for the scattering of $\text{He}(2^3\text{S})$ by H_2 under the assumption of a spherically symmetric H_2 . That is, we assume in this section that the full interaction potentials and width are given only by the v_0^* and Γ_0 terms in the Legendre expansions of the preceding section. That this assumption is reasonable is based on the fact that the higher order terms in Legendre expansions made only a 10% contribution to σ_{ion} at 0.100 eV in the quantum mechanical calculations presented above. However, since the first $[P_0(\cos\theta)]$ term in the Legendre expansion is independent of the angle θ , the problem is thus reduced to one having only a single degree of freedom, R . (The H_2 bond length is still fixed at $r = 1.40 a_0$.) We can thus discuss the problem in the language of an atom-atom collision, which has been thoroughly developed by Miller.¹⁸ The basic aspects of Miller's derivations of the classical cross sections for total and associate ionization are presented in Section 1. Results and comparisons with quantum mechanical calculations and with experiment are presented in Section 2.

1. Theory

The following discussion closely follows Miller's derivations,¹⁸ but employs the notation used in Garrison, Miller, and Schaefer.⁴⁷ We

assume throughout that the total collision energy E is fixed, and that all quantities are given in atomic units. The classical theory of Penning ionization is then formulated in the language of probabilities. For a given impact parameter b , $P_b(R)dR$ is the probability that ionization occurs in the interval $(R, R+dR)$. Then, for a particle approaching with impact parameter b , it can be shown that¹³

$$P_b^{\text{in}}(R) = \frac{\Gamma(R)}{v_b(R)} \exp\left[-\int_R^{\infty} dR' \frac{\Gamma(R')}{v_b(R')} \right] \quad , \quad (5.18)$$

where Γ is the autoionization width and $v_b(R)$ is the radial velocity at R :

$$v_b(R) = \left\{ \frac{2}{m} \left[E - v_0^*(R) - \frac{Eb^2}{R^2} \right] \right\}^{1/2} \quad . \quad (5.19)$$

Since Γ is the ionization rate and $\frac{1}{v_b(R)}$ is roughly the time spent in the interval $(R, R+dR)$, $\Gamma(R)/v_b(R)$ is the probability of ionizing in the interval $(R, R+dR)$. The exponential factor is the survival factor for reaching R without ionizing. Similarly, for a retreating particle,

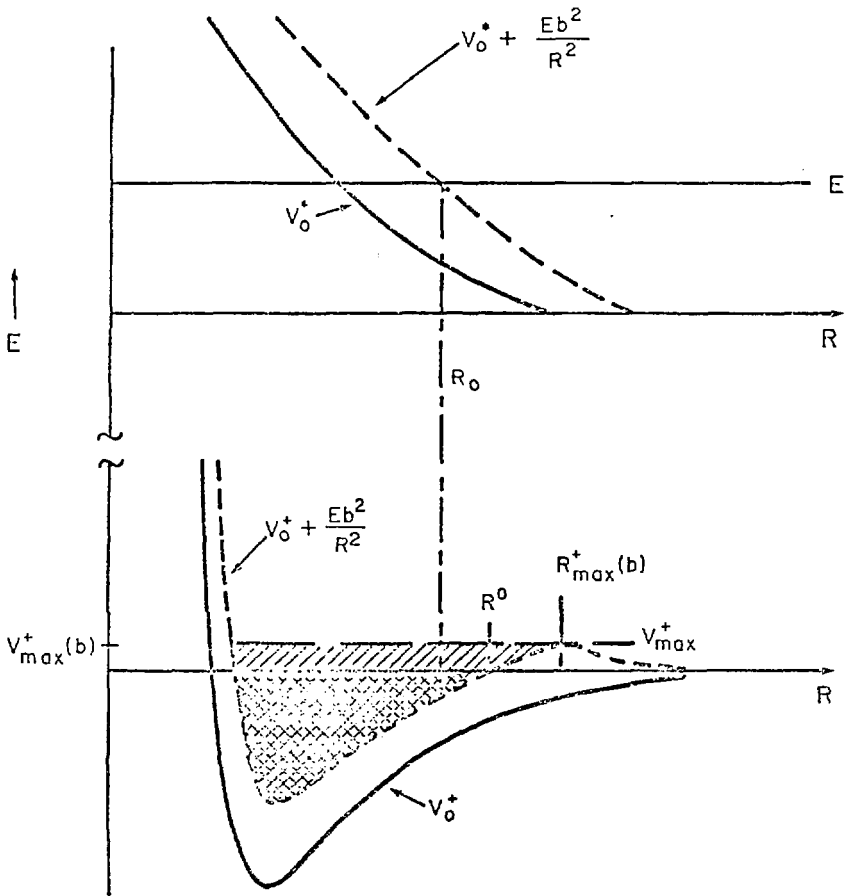
$$P_b^{\text{out}}(R) = \frac{\Gamma(R)}{v_b(R)} \exp\left[-\int_{R_0}^{\infty} dR' \frac{\Gamma(R')}{v_b(R')} - \int_{R_0}^R dR' \frac{\Gamma(R')}{v_b(R')} \right] \quad , \quad (5.20)$$

where R_0 is the classical turning point, i.e., the point for which

$$E = v_0^*(R) + \frac{Eb^2}{R^2} \quad (5.21)$$

(see Figure IX). The total probability for ionization at R is thus given by

Figure IX. Classical potential curve model used for the description of Penning and associative ionization in an atom-atom problem. See text for definitions of indicated quantities.



$$P_b(R) = P_b^{\text{in}}(R) + P_b^{\text{out}}(R) \quad , \quad (5.22)$$

and the total probability for ionization along a trajectory of impact parameter b is simply

$$P_b = \int_{R_0}^{\infty} P_b(R) dR \quad . \quad (5.23)$$

To obtain a total cross section for ionization, we thus need to add up all the contributions from individual impact parameters:

$$\sigma_{\text{tot}} = 2\pi \int_0^{\infty} db \cdot b \cdot P_b \quad . \quad (5.24)$$

Performing the necessary substitutions and the integration over R , we obtain

$$\sigma_{\text{tot}} = 2\pi \int_0^{\infty} db \cdot b \cdot [1 - \exp\{-2 \int_{R_0}^{\infty} dR' \frac{\Gamma(R')}{v_b(R')}\}] \quad . \quad (5.25)$$

We would also like to calculate the amount of associate ionization, i.e., the cross section σ_{AI} for the formation of HeH_2^+ in our atom-atom picture. We can then compute the branching ratio $R = k_{AI}/k_{\text{tot}}$, which can be compared with experiment. Classically, we can consider the ionization as a vertical transition from the excited v_0^* curve to the ionized v_0^+ curve, where the nuclear kinetic energy is locally conserved (see Figure IX). (The v_0^+ curve is just the $\ell = 0$ Legendre moment for the $r = 1.40$ SCF results for V_+ presented in Chapter IV.) If, after the ionization has occurred, the nuclear kinetic energy falls within the shaded region of Figure IX, we have a bound (i.e., associated)

product. This includes both a component which is truly bound (E less than $v_0^+(\infty)$) as well as a component which is only quasibound (E less than the centrifugal barrier). The criteria for deciding if the final nuclear kinetic energy falls within the shaded region can be included by restricting the limits on the R integration of P_b and by multiplying the integrand in Eq. (5.23) by a step function $h(x)$, which equals one if the final energy is sufficiently low and equals zero otherwise. Assuming, as is the case presented here, that the topology of v_0^* and v_0^+ are such that only a single reaction of R contributes to σ_{AI} , we obtain for σ_{AI} a triple integral

$$\sigma_{AI} = 2\pi \int_0^B db \cdot b \cdot \int_{R_0}^{\bar{R}} dR h(X) \frac{\Gamma(R)}{v_b(R)} \exp\left(-\int_{R_0}^{\infty} dR' \frac{\Gamma(R')}{v_b(R')}\right) \cdot \left[\exp\left(\int_{R_0}^R dR' \frac{\Gamma(R')}{v_b(R')}\right) + \exp\left(-\int_{R_0}^R dR' \frac{\Gamma(R')}{v_b(R')}\right) \right] \quad (5.26)$$

where B is the maximum value of b for which $v_0^+ + \frac{Eb^2}{R^2}$ possesses a well, \bar{R} is $R_{\max}^+(b)$ (cf. Figure IX), and X is given by

$$X = v_{\max}^+(b) - E + v_0^*(R) - v_0^+(R) \quad (5.27)$$

For the amount of the truly bound component only, \bar{R} is taken as the point R^0 where

$$v_0^+(R) + \frac{Eb^2}{R^2} = v_0^+(\infty) \quad (5.28)$$

and X becomes

$$X = v_0^+(\infty) - E + v_0^*(R) - v_0^+(R) \quad (5.29)$$

If we let $R'(b)$ be the largest value of R in the interval $(R_0, R_{\max}^+(b))$ or R_0' for which $h(X) = 1$, we can rewrite the triple integral in Eq.

(5.26) as the double integral:

$$\sigma_{AI} = 2\pi \int_0^B db \cdot b \cdot \left\{ \exp\left[-\int_{R_0}^{\infty} dR \frac{\Gamma(R)}{v_b(R)}\right] \right\} \sinh\left[\int_{R_0}^{R'(b)} dR \frac{\Gamma(R)}{v_b(R)}\right] \quad (5.30)$$

In general, the values of R_0 , B , $R_{\max}^+(b)$, and R_0' must be determined numerically. For certain choices of potentials, however, such as those described below, some of these values can be found analytically.

2. Results

The integrations in Eqs. (5.25) and (5.30) were performed with a Simpsons rule procedure. The R integrals pose a problem, however, in that since $v_b(R)$ approaches zero as R approaches R_0 , the integrand is singular at R_0 . Fortunately, this problem can be obviated by a suitable change of integration variable. Letting $x = \sqrt{R_1 - R_0}$, we get the following transformation.

$$\int_{R_0}^{R_1} dR \frac{\Gamma(R)}{v_b(R)} = 2 \int_0^{\sqrt{R_1 - R_0}} dx \frac{\Gamma(R_0 + x^2) \cdot x}{v_b(R_0 + x^2)} \quad (5.31)$$

The integrand is now finite for all x in $[0, \sqrt{R_1 - R_0}]$. However, the integrand has $0/0$ form as $x \rightarrow 0$, so that the limit of the integrand as $x \rightarrow 0$ must be properly determined for evaluation at or near the lower limit of integration. For the choices of potential forms used

here, this can be done by standard limiting procedures involving expansion techniques. With this limiting procedure taken into account, the integrands in Eqs. (5.25) and (5.30) are smooth, well-behaved functions of R and b . In fact, for energies less than 0.500 eV, 20 integration points were sufficient for four-figure accuracy in σ_{tot} . For higher energies, 40 points proved to be enough. A somewhat larger number of points was required for the σ_{AI} calculations. In addition, the infinite limits in Eq. (5.25) were set to about 20.0 for the b and R integrations.

Before presenting the results for the total ionization cross section, a few remarks are in order on how the classical turning point R_0 was obtained in these calculations. Basically, a strictly numerical technique was used. That is, suppose we define the function $f(R)$ by

$$f(R) = v_0^*(R) + \frac{Eb^2}{R} - E \quad . \quad (5.32)$$

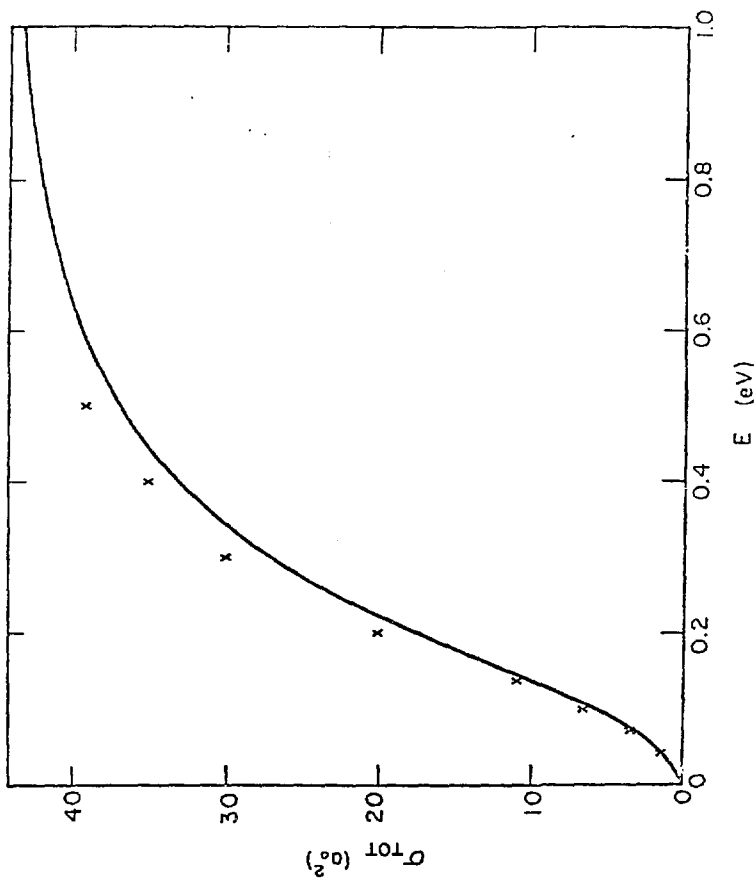
We thus want the value R_0 such that $f(R_0) = 0$. Given the i^{th} approximation to R_0 , we can determine the $(i+1)^{\text{st}}$ approximation by

$$R_{i+1} = R_i - \frac{f(R_i)}{f'(R_i)} \quad . \quad (5.33)$$

Since v_0^* is fit by a cubic spline function, both $f(R_i)$ and $f'(R_i)$ can be determined analytically. Given some initial guess to R_0 then, Eq. (5.33) can easily be iterated until the change in the computed R_0 value between successive iterations is sufficiently small. An efficient method of choosing the initial guess to R_0 is to take the final R_0 value

Figure X. Total ionization cross sections σ_{tot} for $\text{He}(2^3\text{S})+\text{H}_2$ [cf. Eq. (5.25)]. The classical results obtained with an atom-atom approximation (solid curve) are compared with the quantum mechanical results of Section A (crosses).

Figure X.



obtained for the previous value of b . Since the increment between b values was not too large (~ 1), this provided a good initial guess for R_0 . Thus, only the initial guess for $b = 0$ is undetermined. However, for $b = 0$, the condition for R_0 becomes

$$0 = f(R) = v_0^*(R) - E \quad , \quad (5.34)$$

which, since $v_0^*(R)$ is a cubic spline, can be solved analytically.⁴⁸

Also, since E crosses $v_0^*(R)$ at one and only one point in the interval between two cubic fit points, the choice of root is unambiguous.

Results for the total ionization cross section for the collision energy range 0.010 to 1.000 eV are plotted in Figure X, and compared with the quantum mechanical results of Section A. We see that the classical atom-atom results are slightly lower than the quantum ones, but still within 10%. Since the effect of v_2^* in the quantum mechanical calculations was to lower the ionization cross section by around 10%, classical mechanics (i.e., the neglect to tunnelling) appears to introduce roughly a 20% error over quantum mechanics. The magnitude of the error caused by the neglect of tunnelling is reasonable for the case of a repulsive potential and a width which rises rapidly as R decreases. Thermally averaging the cross sections to obtain rate constants as in Eq. (5.17) similarly produced results which are within 10% below those obtained in Section A.

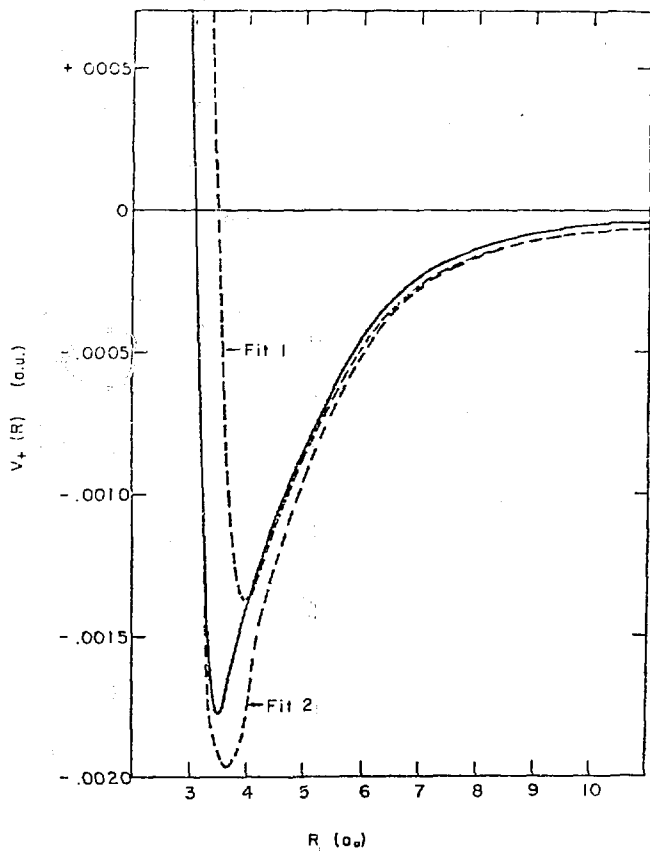
In order to calculate the cross section for associative ionization σ_{AI} , the ionized $v_0^+(R)$ curve is needed. This function was derived from the SCF results for V^+ presented in Chapter IV by the use of Eq. (4.3). It is listed in Table VIII and is plotted in Figure XI. To interpolate between the computed points, the v_0^+

Table VIII. $l = 0$ Legendre moments for V_+ .

$R (a_0)$	v_0^+ (a.u.)
3	+ 0.000642
4	- 0.001381
5	- 0.000833
6	- 0.000439
7	- 0.000231
8	- 0.000129
9	- 0.000076
10	- 0.000050

Figure XI. $l = 0$ Legendre polynomials of the BeH_2^+ potential energy surface (solid curve). The H_2 bond length is fixed at $r_0 = 1.40 a_0$. Fit 1 and Fit 2 (dashed curves) correspond to fits of the form in Eq. (5.35) with $c = 86.826$ and $c = 69.375$, respectively.

Figure XI.



potential was fit by the relatively simple form

$$v_0^+(R) = \frac{c}{R^6} - \frac{c'}{R^4} \quad (5.35)$$

The value of c' was set to 0.69, the polarizability of helium. Taking two different values of c (obtained by a least-squares fit of the data with and without the computed value at $R = 3 a_0$) produced two different fits to v_0^+ , differing primarily in the position and depth of the minimum in the attractive well (cf. Figure XI) and bracketing the correct v_0^+ curve. The true results should thus lie between those obtained from these two fits.

The advantage of using a fit of the form in Eq. (5.35) is that certain upper limits needed in Eq. (5.26) and (5.30) can be determined analytically. The position of the maximum of the centrifugal barrier, R_{\max}^+ (b), and the largest value of b for which $v_0^+(R) + \frac{Eb^2}{R^2}$ contains a well, B , can both be obtained by setting the derivative of the effective potential to zero:

$$0 = \frac{d}{dR} \left(v_0^+(R) + \frac{Eb^2}{R^2} \right) = \frac{1}{R^6} - \frac{c'}{2c} \frac{1}{R^2} + \frac{Eb^2}{R^2} \quad (5.36)$$

As mentioned above, such cubic equations have analytic solutions,⁴⁸ so that R_{\max}^+ (b) is relatively easy to determine. Since no real solutions exist when the discriminant for the equation equals 0, we obtain the condition for B as:

$$B = \frac{[(2/3) c']^{3/4}}{E^{1/2} c^{1/4}} \quad (5.37)$$

R^b , the value for which $v_0^+(R) + \frac{Eb^2}{R^2}$ crosses $v_0^{+(*)}$ (needed for calculating σ_{AI} for truly bound component), can similarly be obtained by solving the cubic equation

$$v_0^+(R) + \frac{Eb^2}{R^2} = 0 \quad (5.38)$$

directly. The final quantity to be determined, $R^1(b)$, corresponding to the largest allowed R value for which the step function $h(X)$ is non-zero, cannot be determined analytically. It was determined by a straightforward numerical search.

Associative ionization cross sections σ_{AI} were calculated with both of the fits given in Figure XI, and with and without the quasibound component. The four sets of cross sections were then thermally averaged via Eq. (5.17), producing associative rate constants k_{AI} at 300°K. From these, branching ratios $R = k_{AI}/k_{tot}$ were computed. Results for the total (both component) associative ionization for Fit 1 and Fit 2 are 16% and 17%, respectively. When just the truly bound component is considered, these results are 12% and 13%. From these results, we can conclude that the branching ratio is not very sensitive to the well region of the ionized curve, which is consistent with the picture that at thermal energies, the particles cannot get much closer than about $5 a_0$. We also note that the quasibound component contributes only 20% to 30% of the branching ratio. However, the experimentally determined branching ratio for the formation of HeH_2^+ is a mere 1.5%.^{32,34} Clearly, some factor has not properly been accounted for in this comparison, since classical mechanics would be expected to underestimate the result, through the neglect of tunnelling. The difference between this

theoretical treatment and what is experimentally determined thus lies in the atom-atom approximation employed here. That is, this model cannot distinguish between true HeH_2^+ and HeH_2^+ which is formed with a sufficient amount of vibrational excitation to subsequently decay to $\text{HeH}^+ + \text{H}$. Since the branching ratio for HeH^+ formation is around 10% at 300°K, this is a plausible explanation. In terms of potential curves, this means that to properly compare with experiment, we need to add the v_2^+ vibrational energy to the v_0^+ curve, thereby raising it relative to the original $v_0^{(c)}$ value and decreasing the size of the well. In fact, for a sufficiently large amount of vibrational energy ($\geq .002$ a.u.), the well would disappear entirely, corresponding to a zero classical cross section for associative ionization. The observed branching ratio for HeH_2^+ formation could then be calculated only in a quantum mechanical framework. This last idea is supported by the work of Preston and Cohen,⁴⁹ who observed no HeH_2^+ formation in a classical trajectory study of this problem.

VI. THE $\text{He}(2^1\text{S})+\text{H}_2$ SYSTEM

This chapter presents the results of our stabilization--golden rule calculations on the $\text{He}(1s1s^1\text{S})+\text{H}_2$ system.⁵⁰ This system is of particular interest in that recent experimental measurements of the differential scattering cross section^{15,16} suggest that, unlike the triplet system, the singlet interaction potential V^* contains a relative maximum (cf. Figure XII). In a previous theoretical study of this system, Cohen and Lane²² found a high degree of anisotropy. However, since their calculation employed a rather limited valence-bond CI wavefunction with a single center expansion for the H_2 orbitals, a reliable maximum was either not observed or not reported.

The method employed in our work was presented in Chapter III. All comments in Chapter IV concerning the procedure and programs apply here as well, and need not be repeated. Only two differences between the work presented in Chapter IV and the current case are significant. First, the orbital basis set listed in Table III was used as given, except that the 2s and 2p orbital exponents on He were changed to 0.505, as determined in a separate calculation of $\text{He}(2^1\text{S})$. Second, unlike the triplet calculation, the ground state (reference) configuration for HeH_2 must be included in the configuration set. Since it was considered a part of the Q subspace of \hat{H} , the root corresponding to resonance was thus the second eigenvalue of $\hat{Q}\hat{H}\hat{Q}$.

The results for the resonance energy V^* are listed in Table IX. Since the singlet SCF calculations on HeH_2^+ differ from the triplet only in the 2s and 2p He exponents, the V_{\perp} results were almost the same as before (differing by 0.0002 a.u.), and need not be repeated.

Figure XII. Interaction potential $V^*(R, \theta)$ for $\text{He}(2^1\text{S}) + \text{H}_2$ (solid curves) with θ fixed at $0^\circ (C_{\infty v})$ and $90^\circ (C_{2v})$. The H_2 bond length is fixed at the equilibrium value $r_0 = 1.40 a_0$. The dashed curve is Haberland's effective spherically symmetric potential (see Reference 30). All curves are plotted with the same zero. The calculated asymptotic limit is $V^*(R \rightarrow \infty, r = 1.40) = -3.273656 \text{ a.u.}$

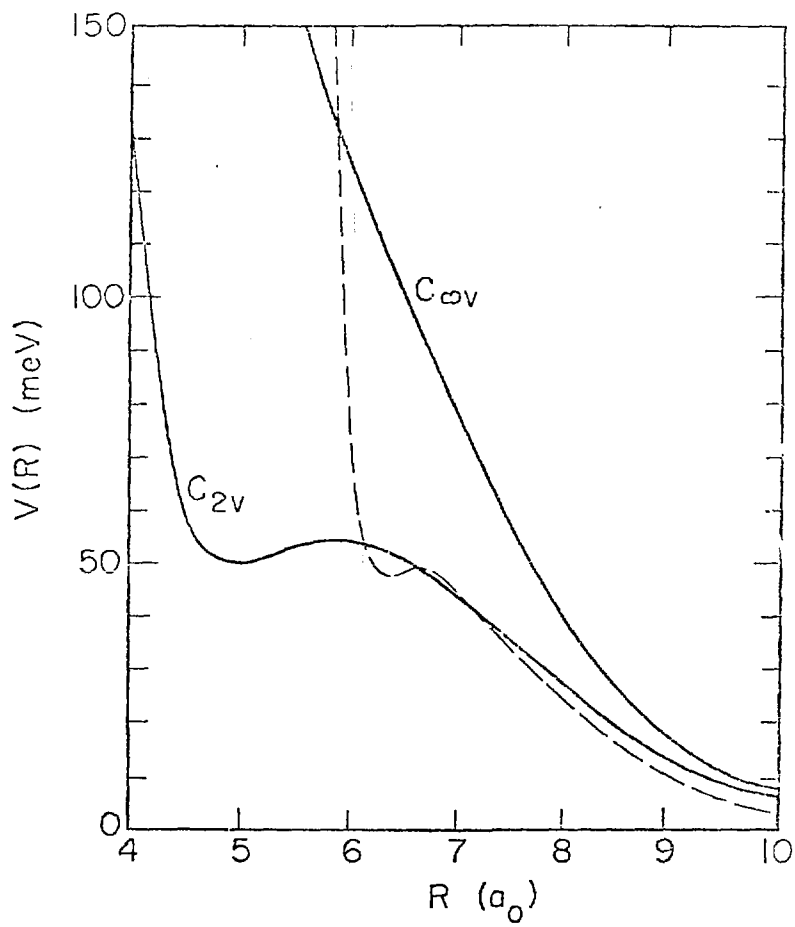


Table IX. Results for the $\text{He}(2^1S)+\text{H}_2$ V^* potential.^a

R	ϕ	r^b	V^*	R	ϕ	r	V^*
3.00	0	1.40	-3.191679	6.00	0	1.40	-3.269032
3.00	45	1.40	-3.216420	6.00	45	1.40	-3.270460
3.00	90	1.40	-3.234810	6.00	90	1.00	-3.222912
4.00	0	1.40	-3.256806	6.00	90	1.40	-3.271680
4.00	45	1.40	-3.263535	6.00	90	1.80	-3.249739
4.00	90	1.40	-3.269144	6.25	0	1.40	-3.269508
4.50	0	1.40	-3.263758	6.25	45	1.40	-3.270702
4.50	45	1.40	-3.267951	6.25	90	1.40	-3.271725
4.50	90	1.40	-3.271489	6.50	0	1.40	-3.269971
4.75	0	1.40	-3.265434	6.50	45	1.40	-3.270956
4.75	45	1.40	-3.268869	6.50	90	1.40	-3.271806
4.75	90	1.40	-3.271769	6.75	0	1.40	-3.270414
5.00	0	1.40	-3.266548	6.75	45	1.40	-3.271217
5.00	45	1.40	-3.269406	6.75	90	1.40	-3.271923
5.00	90	1.40	-3.271817	7.00	0	1.40	-3.270829
5.25	0	1.40	-3.267350	7.00	45	1.40	-3.271479
5.25	45	1.40	-3.269749	7.00	90	1.40	-3.272061
5.25	90	1.40	-3.271776	7.25	0	1.40	-3.271215
5.50	0	1.40	-3.267983	7.50	0	1.40	-3.271571
5.50	45	1.40	-3.770007	7.50	45	1.40	-3.271987
5.50	90	1.40	-3.271714	7.50	90	1.40	-3.272368
5.75	0	1.40	-3.268528	7.75	0	1.40	-3.271890
5.75	45	1.40	-3.270234	8.00	0	1.40	-3.272175
5.75	90	1.40	-3.271677	8.00	45	1.40	-3.272429

Table IX, continued.

R	θ	r	V^*	R	θ	r	V^*
8.00	90	1.00	-3.224158	10.0	90	1.35	-3.273164
8.00	90	1.35	-3.272406	10.0	90	1.40	-3.273431
8.00	90	1.40	-3.262672	10.0	90	1.45	-3.272747
8.00	90	1.45	-3.271987	10.0	90	1.80	-3.251202
8.00	90	1.80	-3.250440	25.0	0	1.40	-3.273657
8.25	0	1.40	-3.272423	25.0	45	1.40	-3.273657
8.50	0	1.40	-3.272638	25.0	90	1.00	-3.225122
8.50	45	1.40	-3.272786	25.0	90	1.35	-3.273388
8.50	90	1.40	-3.272938	25.0	90	1.40	-3.273657
9.00	0	1.40	-3.272978	25.0	90	1.45	-3.272975
9.00	45	1.40	-3.273062	25.0	90	1.80	-3.251443
9.00	90	1.40	-3.273150	50.0	90	1.00	-3.225122
9.50	0	1.40	-3.273217	50.0	90	1.35	-3.273388
9.50	45	1.40	-3.273260	50.0	90	1.40	-3.273656
9.50	90	1.40	-3.273314	50.0	90	1.45	-3.272974
10.0	0	1.40	-3.273381	50.0	90	1.80	-3.251442
10.0	45	1.40	-3.273401				
10.0	90	1.00	-3.224905				

^aAll quantities in atomic units; angles in degrees. The exact asymptotic limit for the potential is $V^*(R \rightarrow \infty, r = 1.40) = -3.3204$ a.u.

^b R , r , and θ are the coordinates defined in Figure II.

Also, the reason that results for the autoionization width are not tabulated will be detailed below. V^* results for a fixed H_2 bond length ($r_0 = 1.49 a_0$) and two fixed orientations ($\theta = 0^\circ$ and $\theta = 90^\circ$) are plotted in Figure XII, and compared with the experimentally deduced potential of Haberland.³⁰ From the figure, we see that the potential is quite anisotropic, and that, whereas the C_{3v} approach is purely repulsive, the C_{2v} approach actually does possess a relative maximum. In addition, a C_s ($\theta = 45^\circ$) approach (not shown) has a pronounced "wiggle", though not a true maximum. Since the potential curve inferred by Haberland³⁰ assumes an isotropic potential, a direct comparison of our results with experiment is not possible. Such a comparison could be made with scattering calculations employing the complex potential $V^* - \frac{i}{2} \Gamma$, but the autoionizing width for this system is not currently available (see below). However, the fact that the height of the relative maximum in our C_{2v} potential is roughly the same as that of Haberland's effective potential³⁰ strongly suggests that our calculation is correctly modeling the physics of the situation.

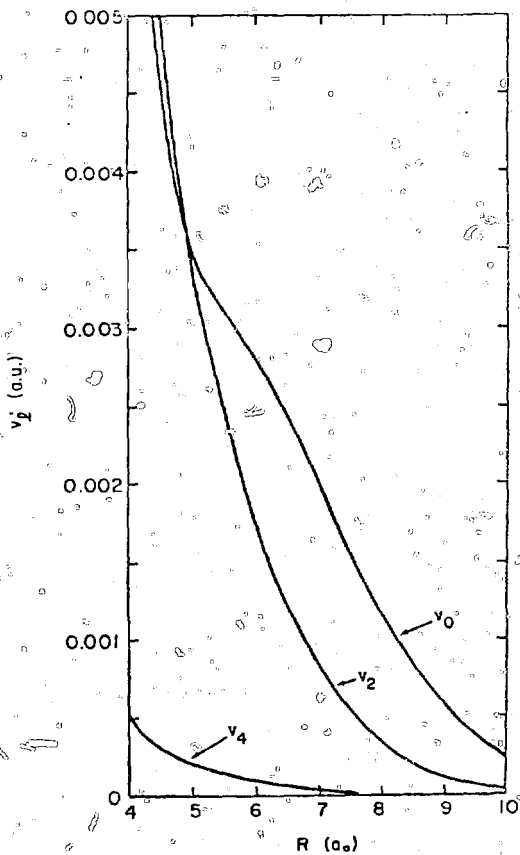
The Legendre moments v_0 , v_2 , and v_4 defined by Eq. (4.1) are plotted in Figure XIII. The large degree of anisotropy is easily visualized from this figure, although the "wiggle" is not very pronounced. In fact, the maximum region in the C_{2v} approach is converged in the Legendre moments to a crossing of the v_0 and v_2 curves. For if $v_0 = v_2$ and v_4 is neglected, it can easily be shown [cf. Eqs. (4.3) to (4.5)] that $V(90^\circ) = \frac{1}{4} V(0^\circ)$, which is nearly true around $R = 5 a_0$.

The physical origin of this unusual structure in the potential does not appear to be due to an avoided crossing with the $He^+ - H_2^-$ ionic state. Such an interaction is precluded by the fact that for the C_{2v}

geometry, the resonance and ionic states are of different spatial symmetries. It should also be pointed out that the structure is not an artifact of our procedure, at least with respect to performing the SCF calculation for the HeH_2^+ state, as the corresponding CI calculation with an SCF on the HeH_2 ground state also produced a C_{2v} curve with a pronounced structure. An analysis of the resonance wavefunction for various R values in the C_{2v} approach indicates that the structure is due to the interaction between two excited states which asymptotically become $\text{He}(1s2s^1S)+\text{H}_2$ and $\text{He}(1s2p^1P)+\text{H}_2$. That is, for R larger than the relative maximum, the excited He electron is in an orbital which has essentially 2s character, while for R inside the maximum, the electron is in an orbital characterized as a 2s-2p_z hybrid. Such s-p correlation was also found to be important to Cohen and Lane.²² To gain a more quantitative view of this hybridization, we performed a crude population analysis, as follows: For fixed R, we consider the eigenvectors for the two roots which dissociate to $\text{He}(2^1S)$, $\text{He}(2^1P)+\text{H}_2$ (roots 2 and 3 of our calculation). For each root, the electron density in the 2s and 2p molecular orbitals of He is then roughly given by the squares of the coefficients for the configurations corresponding to single excitations from the ground state to the respective orbitals. To obtain the atomic orbital densities, these squared coefficients are then multiplied by the proper coefficients of the atomic orbitals in the molecular orbitals, and the results for a given atomic orbital are summed over the 2s and 2p molecular orbitals. We thus end up with a crude measure of the electron density in the excited s and p atomic orbitals, which we can denote by D_s and D_p . We then define the mixing ratio for each of the eigenvectors as D_s/D_p . These mixing ratios are

Figure XIII. Legendre moments $v_l(R)$, $l = 0, 2, 4$, of the $\text{He}(2^1\text{S})+\text{H}_2$ potential energy surface [cf. Eq. (4.1)]. The H_2 bond length is fixed at the equilibrium value $r_0 = 1.40 a_0$.

Figure XIII.



given in Table X. From these results, it is clear that outside the relative maximum, the two roots correspond quite well to distinct S and P excited orbitals, whereas inside the maximum, the two roots become mixed, and at $5 a_0$ the excited orbitals are probably quite nearly sp hybrids.

The structure in the potential surface may now be explained in terms of this s-p hybridization. For the hybridization provides a mechanism whereby electron charge density may be polarized along the R axis and away from the H_2 . Thus, more of the +1 charge of the He^+ core is bared to the H_2 , providing a charge-quadrupole interaction, for which the C_{2v} approach is the most stable. Of course, such an effect is also possible for the $He(2^3S)+H_2$ system discussed in Chapter IV. However, the $He(2^3S)-He(2^3P)$ splitting is 1.14 eV, as opposed to 0.60 eV in the singlet case. Such s-p interaction would then be expected to occur at smaller R values,⁵⁰ where the potential is too steeply repulsive to support a well.

Using the same procedure as was used in the triplet study (see Chapter IV), the autoionization width for $He(2^1S)+H_2$ was computed. Unfortunately, in the present case the width did not fall to zero as the H_2 was moved away ($R \rightarrow \infty$). In fact, Γ reached an asymptotic value of $\sim 10^{-5}$ a.u. To understand the origin of this result, we will restrict our discussion to a C_{2v} geometry with a fixed H_2 bond length of $r_0 = 1.40 a_0$. We also consider the case in which R is large, for in this limit we may talk about molecular orbitals which are centered on either He or H_2 . Since in our calculations the SCF is used to obtain a good set of orbitals with which to describe $He+H_2^+$, in the CI the reference (ground

Table X. D_s/D_p population ratios for $\text{He}(2^1S)+\text{H}_2$.^a

$R (a_0)$	Root 2	Root 3
3	1.07	1.23
4	1.55	1.20
5	2.34	1.01
6	3.66	0.48
7	4.83	0.20
8	1.99	0.66

^aSee text for definitions of quantities involved.

state) configuration, which is in the Q subspace, will mix with the single excitations in the P subspace to provide a better description of H_2 . Unlike the triplet case, then, in which the reference configuration is not included, this normal CI correlation of the H_2 is counted in the H_{PQ} coupling, and thus contributes to the width. Since such correlation would reach some non-zero asymptotic value for large R, Γ would be expected to level off as $R \rightarrow \infty$, as is observed. In addition, since such CI correlation changes with R in some unknown manner, the asymptotic limit cannot simply be subtracted off to provide the width. In fact, when such a procedure is used, the results we obtain are about an order of magnitude smaller than those for the triplet system, in contrast to the results of Cohen and Lane,²² who obtained an approximate singlet width which was slightly larger than their triplet. (Cohen and Lane²² did not observe the correlational difficulties discussed here as they did not use the golden rule approach for their singlet calculations.) It should also be pointed out that these asymptotic difficulties were not observed by Hickman in a golden rule calculation on $He(2^1S)+H$,⁵¹ since as $R \rightarrow \infty$, there is no electronic correlation for the H atom.

In an attempt to remedy our correlation difficulties, we tried a few other schemes, corresponding to different effective choices for the P and Q projectors. First, the reference configuration was removed from the Q subspace and placed in the P subspace, so that the mixing between the ground configuration and the P configurations would not be counted in the width. However, since the reference configuration mixes strongly with the entire Q space, this procedure was not effective. Second, with the reference configuration replaced in the Q subspace, the SCF calculation was performed on HeH_2^+ instead of HeH_2 . This choice

of molecular orbitals provides a poorer description of the continuum function χ in Eq. (3.12), but this is probably not a serious concern, as Cohen and Lane²² obtained reasonable widths for $\text{He}(2^1,^3\text{S})+\text{H}_2$ using quite modest wavefunctions. The advantage of such a choice of molecular orbitals, however, is that by Brillouin's Theorem⁵² we know that the reference configuration cannot mix with those configurations which are single excitations from the reference (i.e., the P configurations). We thus obtained no contributions to the width from the mixing between the reference configuration and the P subspace. However, a different type of correlation in the H_2 was observed in this case. For large R, double excitations in the H_2 (ϵQ) mixed strongly with the single excitations in $\text{H}_2(\epsilon\text{P})$, again providing an asymptotic contribution to the width.

In a final attempt to remove the electronic correlation from the width, we replaced the single determinantal ionic wavefunction ψ_{ion} in χ [cf. Eq. (3.6)] by a three electron CI wavefunction. The idea here is that by "precorrelating" the continuum function χ , the correlational effects described above could be expected to cancel out in the golden rule matrix element of Eq. (3.12). That is, suppose we reconsider the physical approximation assumed for the continuum function χ ,

$$\chi_{\epsilon\ell 0}(\vec{r}_1, \dots, \vec{r}_4) = A\psi_{\text{ion}}(\vec{r}_1, \vec{r}_2, \vec{r}_3)\phi_{\epsilon\ell 0}(\vec{r}_4) \quad , \quad (6.1)$$

where, as before, we expand the coulomb orbital $\phi_{\epsilon\ell 0}$ as

$$\phi_{\epsilon\ell 0}(\vec{r}_4) \sim \sum_{i=1}^n a_i^{(\ell)} \phi_i(\vec{r}_4) \quad . \quad (6.2)$$

However, for $\psi_{\text{ion}}(\vec{r}_1, \vec{r}_2, \vec{r}_3)$, we now take the ground state eigenvector from a CI calculation on HeH_2^+ :

$$\psi_{\text{ion}}(\vec{r}_1, \vec{r}_2, \vec{r}_3) = \sum_k c_k \phi_k^3(\vec{r}_1, \vec{r}_2, \vec{r}_3) \quad , \quad (6.3)$$

where the superscript 3 indicates that ϕ_k^3 is a 3-electron configuration.

We thus obtain for χ :

$$\begin{aligned} \chi_{\epsilon \neq 0} &\cong A \left(\sum_k c_k \phi_k^3 \right) \cdot \left(\sum_i a_i^{(2)} \phi_i \right) \\ &= \sum_i a_i^{(2)} \sum_k c_k \phi_{ik}^4 \quad , \end{aligned} \quad (6.4)$$

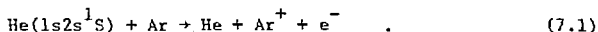
where ϕ_{ik}^4 is a 4-electron configuration corresponding to a proper spatial and singlet spin coupling of the 3-electron configuration ϕ_k^3 with the orbital ϕ_i . ϕ_{ik}^4 can be written as a simple linear combination of configurations ϕ_i for HeH_2 . Assuming that the ϕ_k^3 configurations contain single and double excitations from the 3-electron reference ground state, the ϕ_{ik}^4 will involve linear combinations of single, double, and some triple excitations from the 4-electron reference configuration of the original HeH_2 set. It should be noted here, however, that the only terms in χ of Eq. (6.4) which contribute to the I_Q matrix element of Eq. (4.16) are those terms which were not included in the original Q subspace. To demonstrate this, we assume that a given ϕ_{ik}^4 corresponds to a configuration ϕ_t (or a linear combination of such configurations), where ϕ_t is an element of the Q subspace. Then the contribution to I_Q from the ϕ_{ik}^4 term is related to

$$\begin{aligned}
 \langle \Psi_Q | H - E_T | \Phi_T \rangle &= \langle \sum_j b_j \phi_j | H - E_T | \Phi_T \rangle \\
 &= \sum_j b_j (H_{jT} - H \bar{c}_{jT}) = 0 \quad , \quad (6.5)
 \end{aligned}$$

where the last expression equals zero because the final equality of Eq. (6.5) is simply the secular equation which determines the coefficients $\{b_j\}$ for the eigenvectors of $Q\hat{H}Q$. Contributions to the width only arise, then, from matrix elements between Q configurations and P configurations and between Q configurations and triple excitations from the reference. Unfortunately, both types of matrix elements do not go to zero as $R \rightarrow \infty$, and the results from this procedure are not very different from the original calculation described above, with the exception that the asymptotic limit for Γ is now $\sim 10^{-7}$ a.u. This indicates that a partial cancellation of the correlational effects may be occurring. In conclusion, for cases in which such correlational effects as those presented here are important, the choices of P and Q projectors presented in Chapter III are not suitable for an accurate calculation of the width. A different method presented in Chapter VIII, based on a calculation of the Siegert eigenvalues of a system, shows great promise for the calculation of widths in such cases.

VII. THE He(2^1S)+Ar SYSTEM

Another reaction of current scientific interest is the Penning ionization of Ar atoms by singlet metastable He:^{15-17,53-55}



Haberland¹⁷ recently published an extensive study of the differential elastic scattering cross section for this system at several collision energies, from which it is concluded that a proper calculated fit to the cross section results requires an excited potential V^* which contains a relative maximum (cf. Figure XIV), similar to that observed for the He(2^1S)+H₂ system (cf. Chapter VI). This unusual feature is necessary in that it gives rise to a well-resolved rainbow maximum in the differential cross section observed at intermediate angles (20° for 100 meV). This anomalous rainbow peak has also been observed by Siska,⁵⁵ who obtained the differential cross section at a single collision energy (64 meV). Using a considerably less flexible potential form than that of Haberland, Siska⁵⁵ was able to obtain a good fit to his data with a potential containing a pronounced shoulder (cf. Figure XIV), though not a relative maximum. Nevertheless, the position (7 a₀) and height (25 meV) of the structure in Siska's potential are in good agreement with those of Haberland's. In addition, Siska's time-of-flight measurements⁵⁵ contain a single peak corresponding to elastic scattering, indicating that the observed behavior does not arise from an excitation transfer process producing Ar*.

Since this system has only a single degree of freedom for the nuclear motion, a theoretical calculation of the V^* potential is most

worthwhile, as it can be directly compared with the experimentally deduced potentials. Such a calculation is presented in this chapter. As the number of electrons in the HeAr system (20) is relatively large, extensive CI calculations were not considered feasible. However, the reasonably-sized calculation presented herein, while not of sufficient accuracy to reproduce the exact details of the potential, was considered adequate enough to furnish the gross shape of V^* , i.e., two high-slope regions separated by about $2 a_0$ and joined by a low-slope region.

The calculation of V^* presented in this chapter differs significantly from the method detailed in Chapter III in three respects. First, those configurations corresponding to a HeAr⁺ core plus another orbital (the P subspace of Chapter III) were included in the CI diagonalization. This corresponds to the alternative definitions of the P and Q projectors as used by Miller and Schaefer⁵ in a stabilization calculation for the He^{*}H system. Such definitions place all the L^2 functions of the basis set into the Q subspace, while the P subspace contains only non- L^2 functions. Second, the molecular orbitals from which the configurations were generated were determined by an SCF calculation on the neutral HeAr system, instead of on HeAr⁺. That such a procedure does not change the overall characteristics of the calculated potential was discussed in Chapter VI. Third, all structure calculations discussed in this chapter were performed with the BERKELEY system⁵⁶ of minicomputer-based programs.

The atomic orbital basis set of 34 contracted Gaussian functions used in our study is listed in Table XI. Those orbitals centered on He are the same as those used for the He(2^1S)+H₂ calculations (cf.

Figure XIV. Interaction potentials for $\text{He}(2^1S)+\text{Ar}$ plotted on a linear scale. The solid curve is the theoretical result. The dashed curve is Haberland's deduced potential (cf. Reference 30), while the dot-dashed curve is Siska's deduced potential (cf. Reference 55). All curves are plotted with the same zero. The calculated asymptotic limit is -528.944849 a.u.

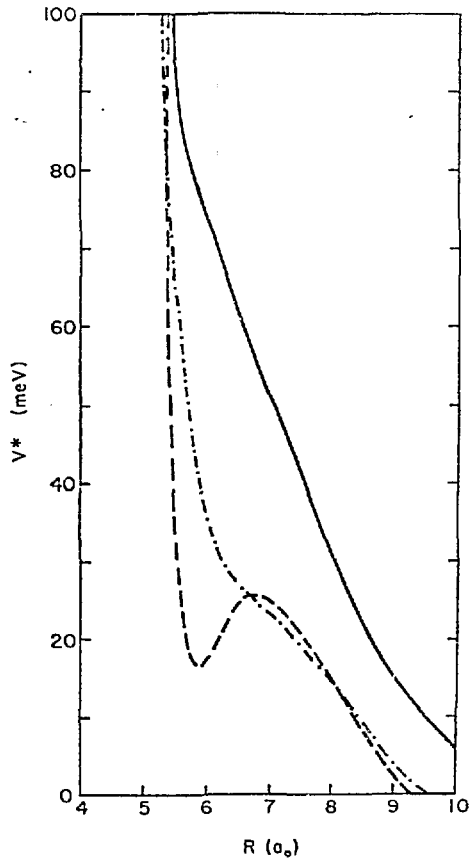


Table XI. Contracted Gaussian orbital basis set for He(2^1S)+Ar.

Atom	Orbital	Exponent	Coefficient
Ar	1s	118186.	0.00030
		17688.8	0.00238
		4637.30	0.01233
		1144.96	0.04908
		376.954	0.15104
		138.070	0.23140
Ar	1s'	138.070	0.10000
		54.9540	0.40780
		23.1650	0.18556
Ar	2s	7.37688	1.0
Ar	2s'	2.92369	1.0
Ar	3s	0.6506603	1.0
Ar	3s'	0.232877	1.0
Ar	4s	0.083348	1.0
Ar	2p _x , 2p _y , 2p _z	660.901	0.00299
		157.219	0.02364
		50.0639	0.10589
		18.6119	0.28567
		7.43692	0.44322
		3.08857	0.30458
Ar	2p _x ', 2p _y ', 2p _z '	1.10267	1.0
Ar	3p _x , 3p _y , 3p _z	0.414763	1.0

Table XI, continued.

Atom	Orbital	Exponent	Coefficient
Ar	$3p_x^1, 3p_y^1, 3p_z^1$	0.145449	1.0
Ar	$4p_x, 4p_y, 4p_z$	0.051006	1.0
Ar	$3d_{xx}, 3d_{yy}, 3d_{zz}$	0.81	
	$3d_{xy}, 3d_{xz}, 3d_{yz}$		
He	1s	92.4121	0.00916
		16.9437	0.04936
		4.74023	0.16854
		1.62840	0.37056
		0.632354	0.41649
		0.260438	0.13033
He	1s'	23.1030	0.00916
		4.23592	0.04936
		1.18506	0.16854
		0.407099	0.37056
		0.158088	0.41649
		0.065110	0.13033
He	2s	7.06036	-0.004151
		1.29480	-0.02067
		0.363866	-0.05150
		0.052034	0.33463
		0.023616	0.56211
		0.011262	0.17130
He	$2p_x, 2p_y, 2p_z$	1.49656	0.00792
		0.390272	0.05144

Table XI, continued.

Atom	Orbital	Exponent	Coefficient
He	2p, cont'd.	0.139643	0.18984
		0.058374	0.40499
		0.026692	0.40124
		0.012619	0.10519

Chapter VI), except that the expansion of the STO's in Gaussians is given explicitly. For the Ar, the (12s,9p) Gaussian set used by Veillard⁵⁷ was contracted to a [6s,4p] set by Dunning's rules.⁵⁸ This "double-zeta" level basis set on Ar was then augmented by diffuse 4s and 4p Gaussians, with exponents chosen by the even-temperedness criterion.⁵⁹ These diffuse functions were included for a better description of either Ar⁻ or Ar* states, as it was felt that such states might play a role in determining the interaction energy. In addition, a 3d set of polarization functions was added to the Ar, with an exponent of 0.81. The final Ar basis of 28 contracted Gaussians gave an SCF energy which was only 0.006 a.u. higher than that obtained by Veillard⁵⁷ with an uncontracted Gaussian set.

For a given nuclear separation (R), the SCF calculation on HeAr thus provided 34 molecular orbitals from which the configurations were generated. With the $1s^2 2s^2 2p^6$ core of Ar and the highest five virtual orbitals frozen out of the configuration generation, all allowed single and double excitations from the ground state reference occupancy yielded a CI basis set of 1398 configurations. An iterative procedure was used to obtain the desired root of the resulting Hamiltonian matrix. This root was identified by considering the molecular orbital populations determined from the eigenvectors. The results for V^* are given in Table XII and are plotted in Figure XIV. Clearly, no "wobble" is obtained, although the potential does appear to be roughly linear in the $6 a_0$ to $8 a_0$ region, with a sharp rise for $R < 6 a_0$. However, when V^* is plotted on a semilog scale, an anomalous feature is readily apparent (cf. Figure XV). For a normal repulsive potential, such a plot would produce a roughly linear curve for the low-energy repulsion

Table XII. Resonance energies for He(2^1S)+Ar.

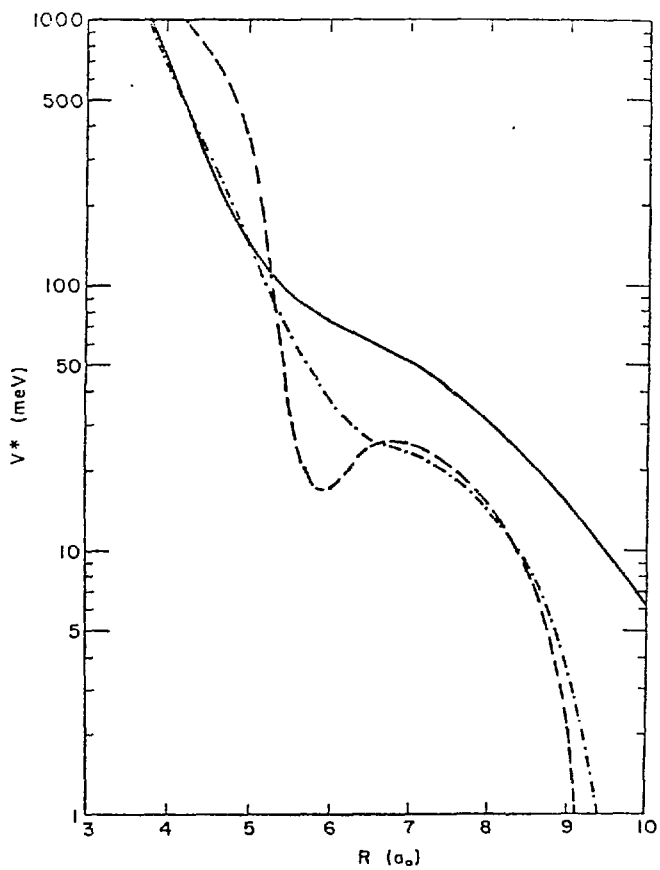
R (a_0)	V^* (a.u.)
4.0	-528.918737
4.5	-528.933942
5.0	-528.939501
5.5	-528.941434
6.0	-528.942164
6.5	-528.942595
7.0	-528.942987
7.5	-528.943373
8.0	-528.943740
8.5	-528.944055
9.0	-528.944308
9.5	-528.944489
10.0	-528.944627
25.0	-528.944849

region. Our calculated V^* curve for $\text{He}(2^1\text{S})+\text{Ar}$, on the other hand, definitely possesses a downward curvature for this region. We also see that the structure in our curve occurs over the same region as the structures in both Haberland's¹⁷ and Siska's⁵⁵ curves, though it is not nearly as pronounced as theirs.

A few more comments on our calculated potential are in order. First, the computed van der Waals tail is too unreliable to be included in our discussion. Second, the computed asymptotic excitation energy for the $\text{He}(2^1\text{S})$ state is 23.6 eV, as opposed to 20.6 eV from experiment. This implies that our calculation is providing a much better description for the ground state of the system than for the excited state under consideration. Third, the calculated asymptotic splitting between the 2^1S and 2^1P states of He is 0.58 eV, in good agreement with the experimental value of 0.60 eV, indicating that the calculation is treating these states equally.

In analogy to the findings of Chapter VI, the anomalous structure obtained here could be expected to arise from the coupling between the two states which dissociate to $\text{He}(2^1\text{S})$, $\text{He}(2^1\text{P})+\text{Ar}$. That is, hybridization of the excited He orbital would allow charge density to be drawn away from the Ar, baring more of the He^+ core to Ar, and lowering the energy. In the present case, we define the s-p mixing ratio as the ratio between the population densities in the 2s and 2p molecular orbitals for the resonant root. (This mixing ratio is somewhat crude, for it does not take into account the s-p hybridization of the molecular orbitals.) These mixing ratios are given as a function of R in Table XIII. We note that the amount of s-p hybridization rises sharply in the

Figure XV. Interaction potentials for $\text{He}(2^1S)+\text{Ar}$ plotted on a logarithmic scale. The solid curve is the theoretical result. The dashed curve is Haberland's deduced potential (see Reference 30), while the dot-dashed curve is Siska's deduced potential (see Reference 55). All curves assume the same zero.



region of the anomalous structure in V^* , but not nearly to the same degree as was observed for $\text{He}(2^1S)+\text{H}_2$. These facts seem to indicate that the same mechanism can be applied to both systems, but that much more extensive calculations need to be performed on He^+Ar to obtain a result which is of comparable accuracy.

In order to determine the extent to which our ab initio potential agrees with the experimentally observed cross sections, we performed quantum mechanical calculations for the differential elastic scattering cross section for $\text{He}(2^1S)+\text{Ar}$, using the single-channel SCAT program provided by Hickman. This program was first tested by reproducing the cross sections obtained by Haberland¹⁷ and Siska⁶⁰ when provided with the potentials and widths^{17,60} those authors found best fit their data. (Note: The A and C coefficients of Haberland's Γ should be corrected⁶¹ to read $A = 1632.6$ eV, $C = 0.0163$ eV.) Our V^* curve was parameterized in the following manner: For R between $4 a_0$ and $10 a_0$, V^* was fit by a cubic spline function through the computed points. For $R > 10 a_0$, V^* was set to $(96.565) \exp(-0.96796 R)$ a.u., while for $R < 4 a_0$, V^* was set to $(766.82) \exp(-1.7460 R)$ a.u. These exponential fits were determined by a fit of the exponential form to the last two and first two computed points, respectively. Regardless of the form assumed for the ionization width Γ , the calculated potential did not yield a differential cross section with a rainbow peak for 100 meV. Instead, a very broad shoulder is obtained, with a breaking angle (i.e., the angle at which $\frac{d\sigma}{d\theta}$ starts to drop precipitously) between 30° and 70° , depending on the form of Γ . This is to be compared with the experimental result of a rainbow peak at 20° for a collision energy of 100 meV. Even

Table XIII. Ratio of P to S character in He(2^1S)+Ar.^a

R (a_0)	Ratio (%)
9.0	0.20
8.5	0.24
8.0	0.60
7.4	1.9
7.0	3.7
6.5	7.3
6.0	12.
5.5	19.
5.0	25.
4.5	29.
4.0	27.

^aSee text for definition of this ratio.

forms for the width containing broad maxima did not change the general shape of the differential cross section. Similarly, addition of the proper van der Waals tail⁶² to our potential did not significantly alter our results. Although it would be useful to compute an ab initio width for the He(2^1S)+Ar system, then, it is doubtful if any such width could provide a differential cross section with a rainbow peak, given our calculated V^* . However, as an anomalous shoulder in the cross section is obtained with our potential, it is possibly fairly close to the accurate one. That is, our potential may need to be modified only slightly (e.g., perhaps made flatter in the $6 a_0$ to $8 a_0$ region) to produce a peaked cross section.

VIII. THE CALCULATION OF SIEGERT EIGENVALUES

In previous chapters, it was demonstrated that the stabilization--golden rule method presented in Chapter III can in some cases be used to obtain reliable positions (E_r) and widths (Γ) for autoionizing systems. In other cases, notably those involving a singlet system which correlates strongly with the ground state, the method was observed to fail in the computation of the autoionization width. In addition, it should be pointed out that the method is an approximate one, not only in the approximation of the continuum function by a function which is square-integrable, but also in the neglect of non-resonant scattering processes. It was thus considered most useful to develop a more exact and direct method to compute E_r and Γ , which could then be applied to molecular problems. As discussed in Chapter I, the aim of such a method is to calculate the complex poles of the S-matrix, or equivalently, of the Green's function, which correspond to resonances. Since the position of such a pole is

$$E = E_r - \frac{i}{2} \Gamma \quad , \quad (8.1)$$

we can directly obtain the position and width of the resonance from the real and imaginary parts of the pole position. This procedure therefore obviates the need for choosing P and Q projectors, and avoids the approximations inherent in the golden rule expression.

As mentioned in Chapter I, one such direct approach, the method of rotated coordinates, has already proven successful for calculations of small atomic systems,¹⁴ e.g., H^- and He^- . However, this method suffers

from the ambiguity (as well as excess computation) of examining the "stability" of the complex eigenvalue with respect to the rotation angle. A more serious drawback with this method is that the extension to non-spherically symmetric systems, i.e., molecules, is unclear. Another direct approach, the one which will be discussed in this chapter, is based on a variational calculation of the Siegert eigenvalues of the system.⁹⁻¹¹ As will be demonstrated below, this approach contains several important advantages: (1) the method requires little more than standard electronic structure techniques, (2) the resulting complex eigenvalues are stable with respect to increasing the size of the basis set, (3) only a relatively small number of diagonalizations must be performed to obtain converged results, (4) the extension to molecular systems is quite straightforward, and (5) no significant approximations are involved.

The method employed in this chapter stems from the variational calculation of Siegert eigenvalues proposed by Bardsley and Junker,¹⁰ and applied by them to a one-dimensional model problem, to the $2s^2$ autoionizing state of H^- , and to the lowest 2S resonance of He^- .¹¹ It will be demonstrated below, however, that Bardsley and Junker's somewhat pessimistic conclusions on the applicability of this method to more complicated systems can be disregarded when a proper iterative scheme to obtain the Siegert eigenvalues is employed. The basic theory of the Siegert eigenvalue approach is presented in Section A, along with the results for a one-dimensional model problem, from which it will become evident that the method converges in a completely stable manner to the correct result as the basis set size is increased.

Section B presents the application of the method to some well-known autoionizing states of H^- and He, and it is demonstrated that results of useful accuracy ($\leq 20\%$ error in \bar{r}) can be obtained with quite modest variational functions (≤ 10 configurations).⁶³ The extension to molecular problems and results for the $He(2^3S)+H$ and $He(2^1S)+H$ systems are presented in Section C.

A. The Variational Calculation of Siegert Eigenvalues

To illustrate the variational calculation employed by Bardsley and Junker¹⁰ to calculate the Siegert eigenvalues of a system, we consider s-wave scattering from a potential $V(r)$ which can support a resonance. We also assume that $V(r)$ is identically zero for $r \geq r_0$. Employing atomic units throughout (and taking $m = 1$ as well), the Schrödinger equation for our problem is given by

$$\left(-\frac{1}{2} \frac{d^2}{dr^2} + V(r) - \frac{1}{2} k^2\right) \psi_k(r) = 0 \quad , \quad (8.2)$$

where $k = \sqrt{2E}$. The usual scattering boundary conditions require that the solutions $\psi_k(r)$ to Eq. (8.2) that we desire be regular at the origin and asymptotically ($r > r_0$) behave like

$$\psi_k(r) \sim e^{-ikr} + S(k) e^{ikr} \quad , \quad (8.3)$$

where $S(k)$ is the S-matrix, which for real k is a number of unit modulus. We then need to look at complex values of k for which $S(k)$ has a pole. The corresponding complex energy $E = \frac{1}{2} k^2$ is a pole of the analytically continued Green's function, and thus

$$E = E_r - \frac{i}{2} \Gamma \quad . \quad (8.4)$$

It can then be shown⁹ that $S(k)$ has a pole at k if and only if

$$\psi_k'(r_0) - ik \psi_k(r_0) = 0 \quad . \quad (8.5)$$

We thus have an eigenvalue problem for Eq. (8.2) with the boundary conditions that $\psi_k(r)$ be regular at the origin and satisfy Eq. (8.5) at $r = r_0$. It is interesting to note that this eigenvalue problem is not Hermitian. The consequences of this fact (e.g., that the eigenvalues need not be real) will be discussed below. Of greater importance is the fact that for physical systems, there is no finite distance r_0 beyond which the potential identically vanishes. We thus need to consider the limit of Eq. (8.5) as $r_0 \rightarrow \infty$. This corresponds to a new asymptotic boundary condition

$$\psi_k(r) \sim \text{constant} \times e^{ikr} \quad , \quad (8.6)$$

which can also be obtained from the usual boundary condition [Eq. (8.3)] by assuming that $S(k)$ has a pole at k . Physically, this indicates that a pole in the S -matrix corresponds to a situation in which there are only outgoing waves, which, as discussed in Chapter I, is the case for an autoionizing state. Our eigenvalue problem for physical systems thus requires a solution to Eq. (8.2) which is regular at the origin and contains only outgoing radial waves for large r .

As in the case of a normal, Hermitian problem, we now wish to transform our non-Hermitian eigenvalue problem into a variational problem. Proceeding as in the usual Raleigh-Ritz variational method,

we choose a trial function ψ_t having a form which imposes the desired boundary conditions:

$$\psi_t(r) = \sum_{n=0}^{N-1} c_n \phi_n(r) + c_N \theta(r) \quad . \quad (8.7)$$

The variational coefficients $\{c_n\}$, $n = 0, 1, \dots, N$ are then determined by requiring that the functional $I[\psi_t]$,

$$I[\psi_t] = \int_0^{\infty} dr \psi_t(r) \left[-\frac{1}{2} \frac{d^2}{dr^2} + V(r) - \frac{k^2}{2} \right] \psi_t(r) \quad , \quad (8.8)$$

be stationary with respect to variations in ψ_t . Before continuing, we note that the radial function on the left side of the integrand in Eq. (8.8) is not complex conjugated. This fact arises naturally from the transformation⁶⁴ of the eigenvalue problem to a variational one, in that otherwise $I[\psi_t]$ would be an infinite quantity for all values of k . The basis functions $\{\phi_n\}$, $n = 0, 1, \dots, N-1$ in Eq. (8.7) are square-integrable functions which vanish exponentially, say, for large r (e.g., Slater orbitals), while the Siegert function $\theta(r)$ is chosen such that it imposes the asymptotic boundary condition, Eq. (8.6):

$$\theta(r) = (1 - e^{-r}) e^{ikr} \quad , \quad (8.9)$$

where the $(1 - e^{-r})$ cutoff factor insures that θ goes to zero at the origin, but still allows θ to have the form of a linear combination of (complex) Slater functions. It should be pointed out that, in general, the functional $I[\psi_t]$ is then formally defined only for $\text{Im}(k) > 0$, for which $\theta(r)$ is also square-integrable. However, we

will see that it is possible to evaluate $I[\psi_{\ell}]$, i.e., to solve the variational problem, for all values of k by the process of analytic continuation from the region where $I[\psi_{\ell}]$ is formally defined. Varying the coefficients $\{c_n\}$, $n = 0, 1, \dots, N$ to make $I[\psi_{\ell}]$ stationary then leads in the standard way to the secular equation for the Siegert eigenvalues:

$$\det[M_{n',n}(k)] = 0, \quad n', n = 0, 1, \dots, N, \quad (8.10)$$

where $M_{n',n}(k)$ is the complex symmetric matrix of $(H - \frac{k^2}{2})$ over the full basis set (i.e., including θ). The matrix elements $M_{n',n}(k)$ depend on k both by the $k^2/2$ term and by the fact that $\theta(r)$ is a function of k . Thus, the resonant eigenvalue $E_i(k)$ obtained from Eq. (8.10) is also a function of k . But, by the definition of k ,

$$E_i(k) - \frac{k^2}{2} = 0 \quad (8.11)$$

must be satisfied for $E_i(k)$ to be the true resonance energy. This leads to the use of some sort of iterative scheme in solving for the true resonance energy. If, following Bardsley and Junker,¹⁰ we write Eq. (8.11) as $k = \sqrt{2 E_i(k)}$ and use the iterative procedure

$$k_{\ell+1} = \sqrt{2 E_i(k_{\ell})}, \quad \ell = 0, 1, 2, \dots, \quad (8.12)$$

then convergence to the correct result is not guaranteed; in fact, we have found cases for which this scheme diverges. The proper way to determine the resonance energy is to solve Eq. (8.11) by a Newton-secant iteration scheme. For all of the systems we have studied, only

a few iterations are needed for convergence.

In general, the matrix elements $M_{n',n}(k)$ when one or both functions is the Siegert function exist only for $\text{Im}(k) > 0$; otherwise, $\psi(r)$ is not an L^2 function. However, the solution to Eq. (8.11) requires a k value with $\text{Im}(k) < 0$. We can remove this difficulty by analytically continuing the matrix elements from $\text{Im}(k) > 0$ to $\text{Im}(k) < 0$. In this way, we determine a unique analytic continuation of the entire problem, as stated in Eq. (8.10), from a region where it is formally defined to a region where it is needed. The analytic continuation of the matrix elements can be accomplished in three ways:

(1) If the matrix elements $M_{n',n}(k)$ are algebraic functions of k for $\text{Im}(k) > 0$, we can simply use this function for all appropriate k , i.e., for $\text{Im}(k) < 0$. For example, consider one of the terms in the overlap integral $\langle \theta | \theta \rangle$:

$$J(k) = \int_0^{\infty} dr e^{2ikr} \quad . \quad (8.13)$$

Clearly, this integral is finite only for $\text{Im}(k) > 0$, for which we have

$$J(k) = \frac{i}{2k} \quad . \quad (8.14)$$

But Eq. (8.14) is finite for all $k \neq 0$; in fact, it is a unique analytic continuation of $J(k)$ to the region $\text{Im}(k) < 0$. We can similarly evaluate all other integrals for $M_{n',n}(k)$, and thus obtain $E_i(k)$, for any k of interest.

(2) If the matrix elements $M_{n',n}(k)$ cannot be evaluated analytically, i.e., the integrals are computed numerically at real values of the

integration variables, we can only obtain $M_{n,n}(k)$ and hence $E_i(k)$ for $\text{Im}(k) > 0$. From a set of $E_i(k)$ values at various k values in the upper half k -plane, however, we can construct a rational fraction fit to $E_i(k)$ which then provides the analytic continuation of $E_i(k)$ to the lower half k -plane, as long as the $E_i(k)$ "surface" is sufficiently smooth.

(3) If the $E_i(k)$ "surface" proves to be sufficiently structured that Method (2) is impractical, we can perform the numerical integration by choosing complex quadrature points, i.e., by rotating the contour on which we do the integration. We can then evaluate the numerical integrals for all k of interest, provided the angle of rotation is sufficiently large.

All three of these methods are equivalent, and all give the same result when they are applicable. Where possible, Method (1) is, of course, preferable, since it allows us to compute $E_i(k)$ for $\text{Im}(k) < 0$ directly. We have implemented each of these methods for the various problems discussed below, and shall comment further on them as they arise.

As an example, we have applied the Siegert eigenvalue method to the problem of s -wave scattering from a one-dimensional barrier potential⁶³

$$V(r) = V_0 r^2 e^{-r} \quad . \quad (8.15)$$

This problem was also considered by Bain, et al.,¹⁷ although their method did not employ a proper iterative scheme to solve Eq. (8.11), and hence proper convergence to the correct energy was not achieved.

No such difficulties were observed in the calculations presented here. For our calculations, we used a basis set of orthonormal generalized Laguerre polynomials⁶⁵

$$\phi_n(r) = \frac{\alpha^{3/2}}{\sqrt{(n+1)(n+2)}} r L_n^{(2)}(\alpha r) e^{-\alpha r/2}, \quad n = 0, 1, \dots, N-1, \quad (8.16)$$

augmented with the Siegert function $\psi(r)$ as given in Eq. (8.9), which must first be orthogonalized to the $\{\phi_n\}$. The kinetic energy matrix elements can all be evaluated analytically, while all the other integrals may be computed by stable recursion formulae or related to a finite hypergeometric series containing only positive terms, which can thus be summed without round-off error. Routines for the evaluation of all matrix elements were provided by Dr. C. W. McCurdy. Diagonalization of the resulting complex Hamiltonian matrix was performed with the EISPACK system of programs.⁶⁶ The entire matrix construction and diagonalization was then used as an input function to a Newton-secant iteration scheme over k , performed with the CZERO routine.⁷⁵

Results for the complex resonance eigenvalue as a function of basis set size, i.e., the number of real basis functions, are shown in Table XIV for the case $V_0 = 7.5$. We see that, as the basis set is increased, there is a well-behaved convergence of the real and imaginary parts of the Siegert eigenvalue to the exact value,¹¹ obtained by a numerical integration of the Schrödinger equation. In addition, the convergence is seen to remain stable even after the basis set is increased far beyond that required for practical convergence. Similar behavior was obtained for a very broad resonance, $E = 1.234209 - 0.187228 i$ a.u., obtained for $V_0 = 2.0$. It should be stressed here that only one Siegert

Table XIV. Resonance position and width ($E_{\text{res}} = E_r - \frac{i}{2} \Gamma$) for the potential $V(r) = 7.5 r^2 e^{-r}$. N is the number of square-integrable basis functions (cf. Eq. (8.6), with $\alpha = 2.0$) used in the expansion of the wavefunction [cf. Eq. (8.7)].

N	E_r	Γ
5	3.40822	.004812
10	3.42706	.022380
15	3.42641	.025596
20	3.42641	.025591
25	3.42638	.025586
30	3.42638	.025553
35	3.42639	.025548
40	3.42639	.025548
45	3.42639	.025549
50	3.42639	.025549
60	3.42639	.025549
70	3.42639	.025549

function has been included in the basis. That is, only one such function is required to impose the proper boundary condition on the trial function.

Before describing our calculations on some physical systems, we note a necessary modification to our procedure for the case in which the outgoing particle experiences an attractive coulomb potential, as occurs in Penning ionization. To satisfy the proper physical boundary condition, we require that the Siegert function have the asymptotic form of an outgoing coulomb wave,⁶⁷

$$\begin{aligned} \phi_k(r) &\sim \exp[ikr + \frac{i}{k} 2\pi(2kr)] \\ &\propto r^{i/k} e^{ikr} \end{aligned} \quad (8.17)$$

We thus replace the Siegert function defined in Eq. (8.9) by

$$\theta(r) = r^{i/k} e^{ikr} (1 - e^{-r})^2 \quad (8.18)$$

for s-wave scattering, where the extra power of the cutoff function insures that $\theta(r) \rightarrow 0$ as $r \rightarrow 0$ at least as fast as r . As pointed out before, though, it is most convenient to keep θ in the form of a linear combination of complex Slaters, so that the integrations required for matrix element evaluations will be possible.

B. The Calculation of Atomic Resonances and Results

This section presents the results for the 2^1S resonance in H^- and the 2^1S and 2^1P autoionizing states of helium.⁶³ The trial function in all three cases is a linear combination of two-electron singlet configurations, ψ_1 , of the form

$$\psi_i(1,2) = \frac{1}{2} [\psi_a(1) \psi_b(2) + \psi_b(1) \psi_a(2)] \cdot [\alpha(1) \beta(2) - \beta(1) \alpha(2)], \quad (8.19)$$

where ψ is a one-electron orbital, and α and β are spin functions.

The bound one-electron orbitals are simple normalized Slater functions

$$\psi_i(\vec{r}) = N_n r^{n-1} e^{-\zeta r} Y_{lm}(\hat{r}), \quad (8.20)$$

with the exception that the 2s orbital is a linear combination of two Slater functions which reproduces the hydrogenic 2s orbital. The exact form of the Siegert orbital depends on the resonance under consideration. The following forms were used:

$$\text{for H}^-(2^1S): \quad \theta(\vec{r}) = \frac{e^{ikr}}{r} (1-e^{-r}) Y_{00}(\hat{r}), \quad (8.21)$$

$$\text{for He}(2^1S): \quad \theta(\vec{r}) = \frac{r^{i/k} e^{ikr}}{r} (1-e^{-r})^2 Y_{00}(\hat{r}), \quad (8.22)$$

$$\text{for He}(2^1P): \quad \theta(\vec{r}) = \frac{r^{i/k} e^{ikr}}{r} (1-e^{-r})^3 Y_{10}(\hat{r}). \quad (8.23)$$

The cutoff function, $(1-e^{-r})$, insures that the Siegert orbital limits properly both as $r \rightarrow 0$ and as $r \rightarrow \infty$. Only one configuration involving the Siegert orbital was employed, i.e., the configuration corresponding to a combination of the Siegert orbital with the ground state of the remaining one-electron target [H(1s) or He⁺(1s)].

Using this configurational basis, the variational calculation to find the resonant eigenvalue $E_i(k)$ was performed using a modification of the atomic configuration interaction program written by Schaefer.¹²

Apart from the conversion to complex variables, the major modification to Schaefer's program involved the evaluation of matrix elements containing the Siegert function. Since this function has the form of a complex Slater with an arbitrary, complex power of r , the one-electron integrals can all be written in terms of the complex Gamma function,⁶⁵ while the two-electron integrals can be expressed in terms of the complex hypergeometric series,⁶⁵ ${}_2F_1(a,b;c;z)$. The resulting complex Hamiltonian matrix was then diagonalized with the EISPACK system of programs.⁶⁶ As a test of the entire calculation, k was set to a purely imaginary number, so that $\theta(r)$ becomes a real, L^2 function. The eigenvalues obtained from this calculation agreed exactly with those from a calculation involving only bound orbitals, with exponents chosen to match those in the first calculation. To obtain converged resonance energies, Eq. (8.11) was then solved by a Newton-secant iteration. At first, $E_1(k)$ was computed directly for each iteration of the search. Later, the calculation was modified so as to compute $E_1(k)$ at a small number of real k points in the region of the correct resonance momentum. The resulting set of eigenvalues was fit to a low order rational fraction, which was then continued to find the solution to Eq. (8.11). This procedure resulted in a significant savings in time with no apparent loss of accuracy.

As a test of both the method and the computation, large scale calculations were performed on the three atomic resonances listed above. The basis sets and results for these calculations are given in Table XV, where the results are also compared to reliable ones obtained from

projection operator techniques. In general, the agreement is quite good in both the positions and the widths. The small discrepancy in the position and width of the $\text{He}(2^1P)$ resonance is probably due to residual correlational effects not handled by the basis set.

Since basis sets large enough to be of comparable accuracy for systems with more than two electrons are not feasible, we next studied the accuracy of results from small basis sets. The results for the best choices of small basis sets are presented in Table XVI, along with the large scale results for comparison. For the S resonances, the positions are quite stable even down to 5 configurations, while the widths remain within 20% of the accurate value down to 8 configurations. It can also be noted that the disagreement in the width is larger for the coulomb resonances than for the plane-wave case. This may indicate that the method depends on how rapidly the eigenfunction reaches its asymptotic form. For the P resonance, removal of d functions causes a sharp change in the position, due to the loss of p-d correlation. Except for this (constant) correlation, the position is again stable down to 5 configurations, and the width also remains within 20% of the accurate value down to 5 configurations. These results suggest that this method can be practically applied to larger systems while still maintaining a useful degree of accuracy.

Some comments on the choices of bound basis sets giving the best small-scale results are in order. Since the 1s function must describe the one-electron core in the Siegert configuration, the 1s exponent was set to $\zeta = 2.0$ (1.0) for $\text{He}(\text{H})$. The 2s and 2p exponents were determined in separate optimization runs involving only the 1s, 2s, and 2p orbitals. The optimum values we obtained for the 2s and 2p exponents were respectively

Table XV. Accurate atomic calculations

System	Basis	Best Result		Comparison Value	
		E_R (a.u.)	Γ (eV)	E_R (a.u.)	Γ (eV)
$H^-(2^1S)$	11s4p3d/72 configs.	-1.14876	0.0469	-1.14878 ^a	0.0472 ^a
$He(2^1S)$	10s5p3d/67 configs.	-1.77767	0.126	-1.77804 ^b	0.125 ^b
$He(2^1P)$	6s9p3d1f/76 configs.	-1.69181	0.0403	-1.69316 ^c	0.037 ^c

a) Reference 73.

b) Reference 11.

c) Reference 74.

Table XVI. Small basis atomic calculations

System	Basis	E_R (a.u.)	Γ (eV)
$H^-(2^1S)$	72 configs.	-.14876	0.0469
	1s-6s,2p/23 configs.	-.14777	0.0522
	1s-5s,2p/17 configs.	-.14776	0.0528
	1s-4s,2p/12 configs.	-.14598	0.0493
	1s-3s,2p/8 configs.	-.14551	0.0542
	1s-2s,2p/5 configs.	-.14315	0.0351
$He(2^1S)$	67 configs.	-.77767	0.126
	1s,2s + 1s'-6s',2p/38 configs.	-.77644	0.151
	1s,2s + 1s'-5s',2p/30 configs.	-.77642	0.151
	1s,2s + 1s'-4s',2p/23 configs.	-.77639	0.151
	1s,2s + 1s'-3s',2p/17 configs.	-.77635	0.150
	1s,2s + 1s'-2s',2p/12 configs.	-.77621	0.149
	1s,2s + 1s',2p/8 configs.	-.77348	0.143
	1s,2s,2p/5 configs.	-.77443	0.188
$He(2^1P)$	76 configs.	-.69181	0.0403
	1s,2s,2p + 2p'-6p'/8 configs.	-.65833	0.0337
	1s,2s,2p + 2p'-5p'/7 configs.	-.65833	0.0333
	1s,2s,2p + 2p',4p'/6 configs.	-.65834	0.0332
	1s,2s,2p + 2p'-3p'/5 configs.	-.65833	0.0341
	1s,2s,2p + 2p'/4 configs.	-.65635	0.0894

0.40 and 0.33 for H^- , 0.93 and 0.81 for $He(2^1S)$, and 0.55 and 0.99 for $He(2^1P)$. For the $H^-(2^1S)$ resonance, reasonable results were obtained by including just the $2s^2$ and $2p^2$ configurations needed to describe the bound state, along with a series of $l s n s$ configurations, where $n s$ represents a diffuse Rydberg-like orbital ($n = 3, 4, 5, 6$; $\zeta = 0.5$). The configurations involving the diffuse orbitals seem to be necessary to represent the background continuum. However, in order to obtain the good results for the width presented in Table XVI, it was also found necessary to include all s - s pairs, i.e., to perform a full CI, among the bound s orbitals. This procedure probably corrects, to some extent, for the limited choice of s functions. For the $He(2^1S)$ resonance, good small-scale results were obtained only when the orbital basis used for H^- was augmented with diffuse $1s$ and $2s$ functions. This is probably due to the increased nuclear charge of helium. Again, a full CI among the s orbitals was required. For the $He(2^1P)$ resonance, just the $2s2p$ configuration was used to describe the bound state, augmented by a series of $l s n p$ ($\zeta = 1.70$) configurations to represent the background continuum. In this case a full CI among all s - p type configurations was not required.

C. The Application to Molecular Systems: Results for He($2^{1,3}S$)+H

As demonstrated above, the variational calculation of Siegert eigenvalues is a most promising approach to the determination of atomic autoionization positions and widths, in that results of useful accuracy can be obtained with quite modest basis sets. In addition, this approach is advantageous in that it is exact within the limits of the basis set employed, it provides stable convergence to the correct result for increasing basis size, it avoids the ambiguity of looking for "stability" of the eigenvalue as the basis set (or rotation angle, in the rotated coordinate method) is varied, and it in principle requires little more than standard electronic structure technology. In this section, we extend the method to molecular problems and present reliable results for the He(2^3S)+H and He(2^1S)+H Penning ionization systems.

Although our procedure was detailed in the preceding sections, it is summarized here for clarity. We choose an atomic trial function ψ_t of the form

$$\psi_t(\vec{r}_1, \dots, \vec{r}_M) = \sum_{i=1}^{N-1} c_i \phi_i(\vec{r}_1, \dots, \vec{r}_M) + c_N \Theta(\vec{r}_1, \dots, \vec{r}_M), \quad (8.24)$$

where $\{\phi_i\}$, $i = 1, \dots, N-1$ are bound, M-electron configurations which decay to zero outside some region of space, while Θ is an M-electron configuration involving a combination of the ground state of the (M-1)-electron system with a function which asymptotically behaves like an outgoing coulomb wave in all directions (the Siegert orbital). The Siegert eigenvalues are then determined by requiring that the functional

$$I[\psi_t] = \int \psi_t^\dagger(\vec{r}_1, \dots, \vec{r}_M) \left(H(\vec{r}_1, \dots, \vec{r}_M) - \frac{k^2}{2} \right) \psi_t(\vec{r}_1, \dots, \vec{r}_M) d\vec{r}_1 \dots d\vec{r}_M \quad (8.25)$$

be stationary with respect to variations in ψ_t . (The conjugate function ψ_t^\dagger is defined by taking the complex conjugate of all spherical harmonics in ψ_t but not of the radial functions.⁶⁸) This leads in the usual way to a secular equation for the coefficients $\{c_i\}$, which when solved yields an eigenvalue $E_i(k)$ which we identify on physical grounds as corresponding to resonance. However, we also need to satisfy the equation

$$E_i(k) - \frac{k^2}{2} = 0 \quad , \quad (8.26)$$

which thus demands an iterative solution for the true resonance energy.

The major practical difficulty in extending this procedure to more complicated (i.e., molecular) systems lies in computing the Hamiltonian matrix elements which involve the Siegert orbital. For the autoionization of a neutral system, this function takes the form

$$\theta_{\ell m}(\vec{r}) = \frac{r^{i/k} e^{ikr}}{r} (1 - e^{-r})^{\ell+2} Y_{\ell m}(\hat{r}) \quad ; \quad (8.27)$$

it thus has the form of a linear combination of complex Slater functions. If the bound orbitals of the basis set are chosen as Gaussian functions, it was found that the resulting matrix elements involving θ cannot be computed analytically. On the other hand, if the bound orbitals of the basis are chosen as Slater functions, all the molecular matrix elements cannot be computed analytically even in the case of a diatomic system. Since numerical integration is thus unavoidable for a molecular calculation, we decided to perform our first molecular calculations on diatomic systems and employ a basis of Slater orbitals. The systems we chose to investigate are the $\text{He}(2^3\text{S})+\text{H}$ and $\text{He}(2^1\text{S})+\text{H}$ Penning ionization reactions.

These particular systems have several desirable qualities: (1) Since they contain only three electrons, extensive electronic structure calculations are feasible. (2) Feshbach projection operator technique results are available for comparison for both systems.^{13,21,51} (3) Sufficient experimental data exists⁶⁹⁻⁷² with which to compare ionization cross section results obtained from the computed potentials and widths.

The main theoretical consideration in extending our procedure to molecular systems is that the problem no longer possesses spherical symmetry. In the language of a partial wave analysis, this means that Siegert orbitals of s,p,d, etc., symmetry can all contribute to the trial function, just as the bound orbitals of those symmetries do. It is important to point out, however, that since the asymptotic form of an outgoing coulomb wave holds in all directions, then the asymptotic boundary condition applies to all partial waves (i.e., to all Siegert orbital symmetries), not just to their sum. By the electron exchange model, the ionized electron is thought to depart from the He atom. Therefore, by centering the Siegert orbitals of Eq. (8.27) on the He, we would expect to need only a few partial waves to adequately describe the resonance. This turns out to be the case.

The only remaining theoretical question is how to define the Siegert configuration. First, we note that only $m = 0$ Siegert orbitals need to be considered for the problems we are studying, as they possess Σ symmetry. Then for each $\theta_\lambda(r)$, $\lambda = 0,1,2, \dots$, we wish to consider configurations which have the form of $\theta_\lambda(r)$ times the remaining 2-electron HeH^+ core. Since the dominant configuration in ψ_{HeH^+} is $1s^2_{\text{He}} + \text{H}^+$, we take for our Siegert configurations those configurations which correspond to an orbital occupancy $\phi_a \phi_b \theta_\lambda$, where ϕ_a and ϕ_b are 1s orbitals on He.

The calculations presented in this section were performed with modified versions of the HETINT and MRINO programs written by Schaefer.¹⁶ Since all integrals were performed numerically, it was not necessary to determine analytic expressions for the integrals involving the Siegert functions. The program was then tested in two ways: (1) the $\text{He}(2^1S)$ resonance results of Section B were reproduced by this program; (2) setting k to a pure imaginary number gave the same results as the corresponding bound calculation.

As pointed out in Section A, the form of the Siegert function is such that the numerical integrals cannot in general be evaluated at $\text{Im}(k) < 0$, where Eq. (8.26) has the root we desire. To get around this problem, we first performed the calculation of $E_1(k)$ for $\text{Im}(k) \gg 0$, fit the results to a rational fraction, and attempted to analytically continue this fitted function to the region $\text{Im}(k) < 0$. Unlike the atomic case, however, the $E_1(k)$ "surface" proved to be too structured in the region of k -space for which the numerical integrals were converged for this procedure to be practical. A much more useful approach was to perform the numerical integration along a rotated contour. That is, if a function $f(z)$ is analytic in the upper half z -plane, say, then the integral $\int_0^\infty dx f(x)$ along the real axis is equivalent to the integral along a ray of angle α in the complex plane:

$$\int_0^\infty dx f(x) = \int_0^\infty e^{i\alpha} dz f(z) = e^{i\alpha} \int_0^\infty dx f(xe^{i\alpha}) \quad . \quad (8.28)$$

Since the HETINT program²⁰ performs the numerical integrations in ellipsoidal coordinates (ξ, η) , only the ξ integrations (on the interval $[1, \infty)$) need to be performed on a rotated contour, which is defined by

$$z = (\xi-1)e^{i\alpha} + 1 \quad . \quad (8.29)$$

For real values of k (which proved to be close enough to the true k for our calculations), a rotation angle $\alpha \sim 0.15 \pi$ radians produced integrals with an error of $\leq 10^{-8}$ a.u.

The set of bound, Slater type orbitals used in the calculations presented here is given in Table XVII. This is the same basis as that used by Hickman, et al.²¹ in a golden rule calculation of $\text{He}(2^3\text{S})+\text{H}$, except that the Π orbitals are not included. The orbital basis was then augmented with Siegert functions θ_2 of s, p, and d symmetry centered on He. Since the change in the final Γ was less than 20% upon addition of θ_d , the inclusion of these three Siegert orbital symmetries was considered sufficient. For the CI calculation, all $2\bar{L}$ configurations arising from the bound orbitals (240) were retained. To this set, 4 Siegert configurations were added for each Siegert orbital symmetry. These configurations have the form $\phi_a \phi_b \theta_2$ where ϕ_a and ϕ_b are the $1s$ and/or $1s'$ functions on He. The final CI calculation was thus performed with 252 configurations. As the real resonance energies at each inter-nuclear separation had already been computed for our systems by the stabilization technique,¹³ we could easily determine an approximate value for the real part of the true complex resonance momentum. The resonant eigenvalue $E_i(k)$ was then computed for five closely-spaced real k points bracketing this approximate value. The five resulting $E_i(k)$ values were fit to a low-order rational fraction, which was then analytically continued to the region $\text{Im}(k) < 0$ and the root Eq. (8.26) was found by a Newton-secant search.

The results for the real resonance energies as functions of the

Table XVII. Basis set of Slater orbitals for He($2^1, 3^3S$)+H.^a

Atom	Orbital	Exponent
He	1s	2.0
	1s'	1.0
	2s	0.90
	2s'	0.61 (0.505) ^a
	2p _z	2.0
	2p' _z	0.61 (0.505)
H	1s	1.50
	1s'	1.00
	2p _z	1.00

^aDifferent exponents for the singlet case given in parenthesis.

Figure XVI. Potential curves for $\text{He}(2^1S)+\text{H}$. The solid curve is the present result, obtained from the real parts of the Siegert eigenvalues for various values of R . The dashed curve was obtained by the stabilization method (see Reference 13). The corresponding asymptotic limits are indicated by arrows.

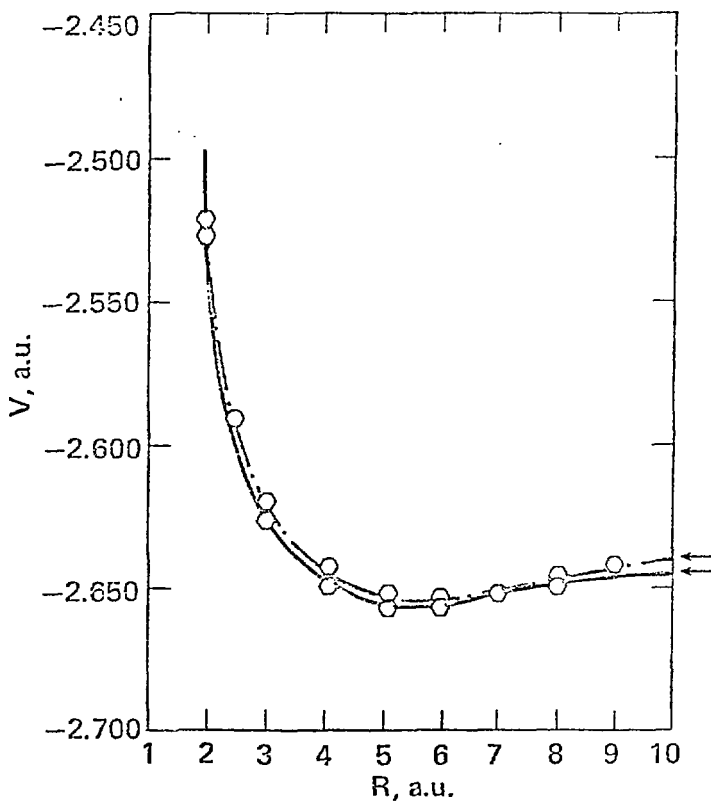


Figure XVII. Potential curves for $\text{He}(2^3\text{S})+\text{H}$. The solid curve is the present result, obtained from the real parts of the Siegert eigenvalues for various values of R . The other curves were obtained by the stabilization method. The dashed curve was taken from Reference 21, while the dot-dashed curve was taken from Reference 13. The corresponding asymptotic limits are indicated by arrows.

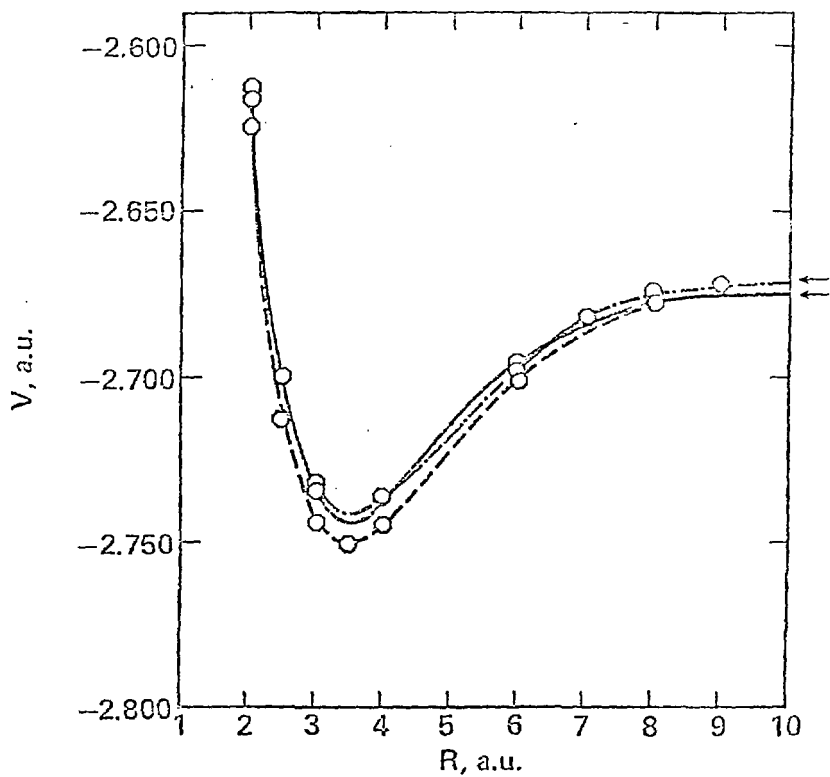


Table XVIII. Autoionization width Γ for He(2^1S)+H.

R (a ₀)	Γ (a.u.)
2.0	1.63×10^{-3}
3.0	2.70×10^{-3}
4.0	1.53×10^{-3}
5.0	4.52×10^{-4}
6.0	8.86×10^{-5}
8.0	$< 10^{-5}{}^a$

^aImaginary part of resonance eigenvalue was below the accuracy level of the calculation.

Table XIX. Autoionization width Γ for $\text{He}(2^3S)+\text{H}$.

R (a_0)	Γ (a.u.)
2.0	8.56×10^{-3}
3.0	3.14×10^{-3}
4.0	8.12×10^{-4}
5.0	1.88×10^{-4}
6.0	5.41×10^{-5}
8.0	2.17×10^{-6}

Figure XVIII. Autoionization widths Γ for $\text{He}(2^1\text{S})+\text{H}$. The solid curve is the present result, obtained from the imaginary parts of the Siegert eigenvalues for various values of R . The dashed curve was obtained by the golden rule method (see Reference 51). The dashed extension of the solid curve is an assumed result, as the imaginary part of the Siegert eigenvalues for $R = 8 a_0$ was below the limit of accuracy for the calculation.

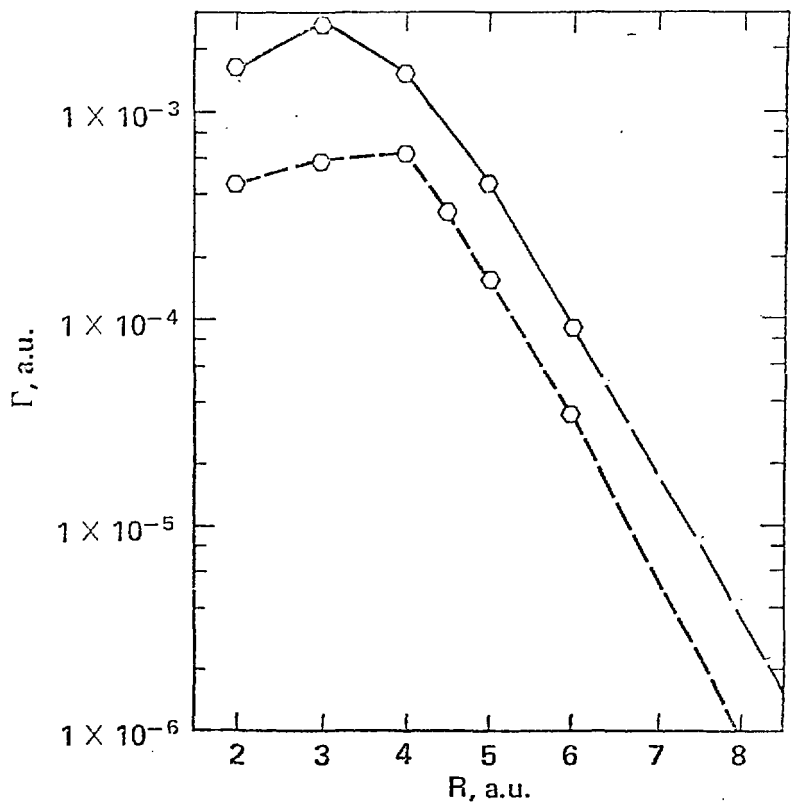
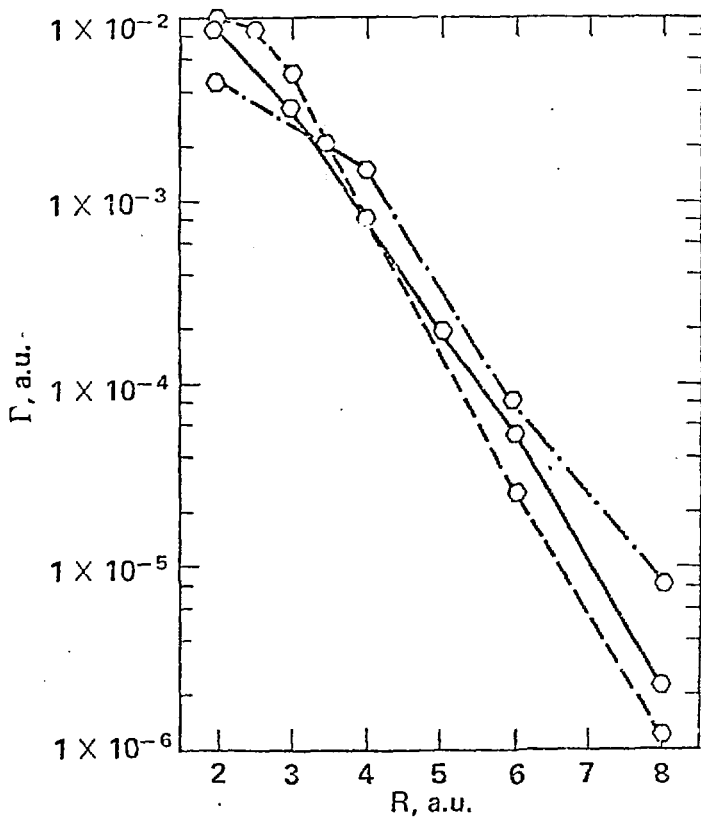


Figure XIX. Autoionization widths Γ for $\text{He}(2^3\text{S})+\text{H}$. The solid curve is the present result, obtained from the imaginary parts of the Siegert eigenvalues for various values of R . The other curves were obtained by the golden rule method. The dashed curve was taken from Reference 51, while the dot-dashed curve was taken from Reference 13.

Figure XIX.



internuclear separation (i.e., the potential curves) are plotted in Figures XVI and XVII for the singlet and triplet systems, respectively, and are compared with the results from the stabilization technique.^{13,21} We see that in both cases the general agreement is quite good. Results for the singlet and triplet ionization widths as functions of R are listed in Tables XVIII and XIX, respectively. These results are also plotted in Figures XVIII and XIX and compared with the golden rule results of Miller, Slocomb, and Schaefer¹³ and Hickman and Morgner.⁵¹ For the triplet case, our width agrees well with both golden rule calculations, although it seems to favor the results of Hickman, et al.²¹ For the singlet system, our width is somewhat larger than Hickman's.⁵¹ Both calculations, however, contain a maximum in the width at about $3 a_0$. Hickman⁵¹ was able to attribute this to a maximum in the density of states factor in the golden rule expression (see Chapter I). It is interesting that we also obtain this maximum, even though the density of states does not appear explicitly in our calculations. In addition, Hickman⁵¹ found that to obtain good agreement between his calculated ionization cross section results and those of experiment,⁷² his width would have to be increased by about a factor of 2.5. Since our results are between a factor of 2 and 3 larger than Hickman's for $R \geq 4 a_0$, we feel confident that cross sections calculated from our potential and width would be in very good agreement with experiment. We therefore conclude that a variational calculation of the Siegert eigenvalues of a system provides an efficient and accurate method of determining the positions and widths of molecular resonances.

ACKNOWLEDGMENTS

I wish to express my sincere gratitude to Professor William H. Miller for his encouragement and guidance throughout my graduate training. I am also most grateful to Professor Henry F. Schaefer III for assistance in choosing the HeAr basis set, as well as for providing the original structure programs with which the Siegert calculations were performed. I am indebted to Dr. Keiji Morokuma for providing the CI code used in the triatomic calculations, and to Dr. Richard Jaffe for assistance in implementing it. In addition, I wish to express special thanks to Drs. A. Peet Hickman and C. William McCurdy for highly rewarding collaborations.

This work was supported by the Division of Chemical Sciences, Office of Basic Energy Sciences, U. S. Department of Energy.

REFERENCES

1. U. Fano, Phys. Rev. 124, 1866 (1961).
2. A. U. Hazi and H. S. Taylor, Phys. Rev. A 1, 1109 (1970).
3. A. U. Hazi and M. F. Fels, Chem. Phys. Lett. 8, 582 (1971); M. F. Fels and A. U. Hazi, Phys. Rev. A 4, 662 (1971); 5, 1236 (1972).
4. H. S. Taylor and L. D. Thomas, Phys. Rev. Lett. 28, 1091 (1972).
5. W. H. Miller and H. F. Schaefer III, J. Chem. Phys. 53, 1421 (1970).
6. W. H. Miller, Chem. Phys. Lett. 4, 627 (1970).
7. H. Feshbach, Ann. Phys. 5, 357 (1958).
8. H. S. W. Massey, E. H. S. Burhop, and H. B. Gilbody, Electronic and Ionic Impact Phenomena, Vol. I, (Clarendon Press, Oxford, 1969).
9. A. J. F. Siegert, Phys. Rev. 56, 750 (1939).
10. J. N. Bardsley and B. R. Junker, J. Phys. B 5, L178 (1972).
11. R. A. Bain, J. N. Bardsley, B. R. Junker, and C. V. Sukumar, J. Phys. B 7, 2189 (1974).
12. A. K. Bhatia and A. Temkin, Phys. Rev. A 11, 2018 (1975).
13. W. H. Miller, C. A. Slocomb, and H. F. Schaefer III, J. Chem. Phys. 56, 1347 (1972).
14. J. Nuttall and H. L. Cohen, Phys. Rev. 188, 1542 (1967); S. B. Raju and G. D. Doolen, Phys. Rev. A 9, 1956 (1970); G. D. Doolen, J. Nuttall, and R. W. Stagat, Phys. Rev. A 10, 1612 (1974).
15. M. T. Leu and P. E. Siska, J. Chem. Phys. 60, 2179, 4082 (1974).
16. B. Brutschy, H. Haberland, H. Morgner, and K. Schmidt, Phys. Rev. Lett. 36, 1299 (1976).
17. H. Haberland and K. Schmidt, J. Phys. B 10, 695 (1977).
18. W. H. Miller, J. Chem. Phys. 52, 3563 (1970).

19. A. P. Hickman, A. D. Isaacson, and W. H. Miller, Chem. Phys. Lett. 37, 63 (1976).
20. H. F. Schaefer III, J. Chem. Phys. 52, 6241 (1970).
21. A. P. Hickman, A. D. Isaacson, and W. H. Miller, J. Chem. Phys. 66, 1483 (1977).
22. J. S. Cohen and N. F. Lane, J. Chem. Phys. 66, 586 (1977).
23. K. Morokuma and H. Kanishi, J. Chem. Phys. 55, 402 (1971); S. Iwata and K. Morokuma (to be published).
24. W. Kolos and C. C. J. Roothaan, Rev. Mod. Phys. 32, 219 (1960).
25. J. W. Steed, Ph.D. thesis, University of Manchester (1967); A. R. Barnett, D. H. Feng, J. W. Steed, and L. J. B. Gilfarb, Computer Phys. Commun. 8, 377 (1974).
26. C. Edmiston, J. Doolittle, K. Murphy, K. C. Tang, and W. Willson, J. Chem. Phys. 52, 3419 (1970).
27. W. J. Hehre, W. A. Lathan, W. A. Ditchfield, M. D. Newton, and J. A. Pople, Quantum Chemistry Program Exchange, Indiana University (1973).
28. W. J. Hehre, R. F. Stewart, and J. A. Pople, J. Chem. Phys. 51, 2657 (1969).
29. P. J. Brown and E. F. Hayes, J. Chem. Phys. 55, 922 (1971).
30. R. Altpeter, H. Haberland, W. Konz, P. Oesterlin, and K. Schmidt, J. Chem. Phys. 67, 836 (1977).
31. H. Hotop and A. Niehaus, Z. Phys. 215, 395 (1968).
32. H. Hotop, A. Niehaus, and A. L. Schmeltekopf, Z. Phys. 229, 1 (1969).
33. R. H. Neynaber and G. D. Magnuson, J. Chem. Phys. 61, 749 (1974).
34. W. P. West, T. B. Cook, F. B. Dunning, R. D. Rundel, and R. F. Stebbings, J. Chem. Phys. 63, 1237 (1975).

35. L. T. Specht, K. D. Foster, and E. E. Muschlitz, Jr., J. Chem. Phys. 63, 1582 (1975).
36. A. P. Hickman, A. D. Isaacson, and W. H. Miller, J. Chem. Phys. 66, 1492 (1977).
37. W. Lindinger, A. L. Schmeltekopf, and F. C. Fehsenfeld, J. Chem. Phys. 61, 2890 (1974).
38. A. M. Arthurs and A. Dalgarno, Proc. R. Soc. London 256, 540 (1960).
39. N. F. Mott and H. S. W. Massey, The Theory of Atomic Collisions (Clarendon, Oxford, 1965), 3rd ed., p. 184.
40. H. Fujii, H. Nakamura, and M. Mori, J. Phys. Soc. Jpn. 29, 1030 (1970).
41. A. P. Hickman and H. Morgner, J. Phys. B 9, 1765 (1976).
42. T. F. O'Malley, Phys. Rev. 150, 14 (1966).
43. A. P. Hickman, Ph.D. thesis, Rice University, Houston, Texas (1973).
44. L. L. Barnes, N. F. Lane, and C. C. Lin, Phys. Rev. Sect. A 137, 388 (1965).
45. N. F. Mott and H. S. W. Massey, Phys. Rev. Sect. A 137, 371 (1965).
46. M. S. Child, Molecular Collision Theory (Academic Press, London, 1974), p. 98.
47. B. J. Garrison, W. H. Miller, and H. F. Schaefer III, J. Chem. Phys. 59, 3193 (1973).
48. K. L. Nielsen, College Mathematics (Barnes & Noble, New York, 1958), p. 164.
49. R. K. Preston and J. S. Cohen, J. Chem. Phys. 65, 1589 (1976).
50. A. D. Isaacson, A. P. Hickman, and W. H. Miller, J. Chem. Phys. 67, 370 (1977).

51. A. P. Hickman and H. Morgner, J. Chem. Phys. 67, 5484 (1977).
52. L. Brillouin, Les Champs "Self-Consistent" de Hartree et de Fock (Actualités Sci. Ind. No. 159), Hermann & Cie, Paris (1934); R. K. Nesbet, Proc. R. Soc. London, Ser A 230, 312 (1955).
53. C. H. Chen, H. Haberland, and Y. T. Lee, J. Chem. Phys. 61, 3095 (1974).
54. A. Pesnelle, G. Watel, and C. Manús, J. Chem. Phys. 62, 3590 (1975).
55. R. M. Jordan, D. W. Martin, and P. E. Siska, J. Chem. Phys. 67, 3392 (1977).
56. R. R. Lucchese, B. R. Brooks, J. M. Meadows, W. C. Swope, and H. F. Schaefer, J. Comput. Phys. 26, 243 (1978).
57. A. Veillard, Theoret. Chim. Acta (Berl.) 12, 405 (1968).
58. T. H. Dunning, Jr., Chem. Phys. Lett. 7, 423 (1970).
59. R. C. Raffanetti, J. Chem. Phys. 58, 4452 (1973).
60. P. Siska, private communication.
61. H. Haberland, private communication.
62. K. L. Bell, A. Dalgarno, A. E. Kingston, J. Phys. B 2, 18 (1968).
63. A. D. Isaacson, C. W. McCurdy, and W. H. Miller, submitted to Chem. Phys.
64. P. L. Kapur and R. Peierls, Proc. Roy. Soc. A, 166, 277 (1938).
65. M. Abramowitz and I. Stegun, Handbook of Mathematical Functions (U.S. Gov't Printing Office, Washington, 1964).
66. EISPACK system, National Energy Software Center, Argonne, Ill., July 1975.
67. A. Messiah, Quantum Mechanics (John Wiley & Sons, New York, 1961), Chapter XI.

68. A. Herzenberg and F. Mandl, Proc. Roy. Soc. A 274, 256 (1963).
69. J. Fort, J. J. Laucagne, A. Pesnelle, and G. Watel, Chem. Phys. Lett. 37, 60 (1976).
70. J. Fort, J. J. Laucagne, A. Pesnelle, and G. Watel, Phys. Rev. A 14, 658 (1976).
71. H. Morgner, Doktorarbeit, Universität Freiburg, 1976.
72. G. D. Magnuson and R. H. Neynaber, J. Chem. Phys. 60, 3385 (1974);
R. H. Neynaber and G. D. Magnuson, J. Chem. Phys. 62, 4953 (1975).
73. Y. K. Ho, A. K. Bhatia, and A. Temkin, Phys. Rev. A 15, 1422 (1977).
74. A. K. Bhatia, P. G. Burke, and A. Temkin, Phys. Rev. A 8, 21 (1974).
75. Subroutine CZERO, Robert Mathews, Lawrence Berkeley Laboratory Computer Center Source Library, Jan. 1971.